FINAL REPORT

Understanding Shipboard Oil/Water Emulsions Using Macro- and Micro-scale Flows

SERDP Project WP18-1031

DECEMBER 2020

Cari Dutcher
University of Minnesota, Twin Cities

SERDP
DOD ▪ EPA ▪ DOE

REPORT DOCUMENTATION PAGE

Form Approved
OMB No. 0704-0188

1. REPORT DATE *(DD-MM-YYYY)*	**2. REPORT TYPE**	**3. DATES COVERED** *(From - To)*
11/12/2020	SERDP Final Report	3/29/2018 - 3/30/2021

4. TITLE AND SUBTITLE

Understanding Shipboard Oil/Water Emulsions Using Macro- and Micro-scale Flows

5a. CONTRACT NUMBER
18-C-0024

5b. GRANT NUMBER

5c. PROGRAM ELEMENT NUMBER

6. AUTHOR(S)
Cari Dutcher

5d. PROJECT NUMBER
WP18-1031

5e. TASK NUMBER

5f. WORK UNIT NUMBER

7. PERFORMING ORGANIZATION NAME(S) AND ADDRESS(ES)
University of Minnesota, Twin Cities
111 Church St. SE
111 Mechanical Engineering
Minneapolis, MN 55455

8. PERFORMING ORGANIZATION REPORT NUMBER
WP18-1031

9. SPONSORING/MONITORING AGENCY NAME(S) AND ADDRESS(ES)
Strategic Environmental Research and Development Program (SERDP)
4800 Mark Center Drive, Suite 16F16
Alexandria, VA 22350-3605

10. SPONSOR/MONITOR'S ACRONYM(S)
SERDP

11. SPONSOR/MONITOR'S REPORT NUMBER(S)
WP18-1031

12. DISTRIBUTION/AVAILABILITY STATEMENT
DISTRIBUTION STATEMENT A. Approved for public release: distribution unlimited.

13. SUPPLEMENTARY NOTES

14. ABSTRACT
The objective of this work is to enhance the “fundamental knowledge base” of the “generation, stabilization and worsening” shipboard oil/water emulsions in the presence of complex, yet tunable, hydrodynamic fields with varied chemical conditions (quotes from SERDP Statement of Need, SON). The separation of emulsified oil from bilge waters poses a unique challenge due to the inherent complexity and stability of these oil/water emulsion systems. Comprehensive scientific analysis of shipboard emulsions is needed to facilitate appropriate water treatment necessary for proper disposal. It is hypothesized here that by studying the oil-in-water system on length and time scales relevant to shipboard chemical composition and treatment processes, new insights into dynamics of shipboard emulsions is possible,

15. SUBJECT TERMS
Emulsion, bilgewater, droplets, surfactants, microfluidics, interfacial tension, coalescence, film drainage, isotherm models, Taylor-Couette flow

16. SECURITY CLASSIFICATION OF:			**17. LIMITATION OF ABSTRACT**	**18. NUMBER OF PAGES**	**19a. NAME OF RESPONSIBLE PERSON**
a. REPORT	**b. ABSTRACT**	**c. THIS PAGE**			Cari Dutcher
UNCLASS	UNCLASS	UNCLASS	UNCLASS	58	**19b. TELEPHONE NUMBER** *(Include area code)* 612-624-0428

Table of Contents

List of Figures

List of Tables

List of Acronyms

SON – Statement of Need
CMC – Critical micelle concentration
IFT – Interfacial Tension
NSBM#4 –Oil Phase Mixture in Simulated Bilgewaters (Defined in Table 1)
AES – Alcohol Ethoxy Sulfate
LAS – Linear Alkylbenzene Sulfonate
LMO – Light Mineral Oil
PMDS – Poly Dimethylsiloxane
SSW – Synthetic Sea Water
TC – Taylor Couette

Keywords

Emulsion, bilgewater, droplets, surfactants, microfluidics, interfacial tension, coalescence, film drainage, isotherm models, Taylor-Couette flow

Acknowledgements

This material is based upon work supported by the Humphreys Engineer Center Support Activity under Contract No. W912HQ18C0024, SERDP project WP18-1031. Any opinions, findings and conclusions or recommendations expressed in this material are those of the author(s) and do not necessarily reflect the views of the Humphreys Engineer Center Support Activity. Portions of this work were conducted in the Minnesota Nano Center, which is supported by the National Science Foundation through the National Nano Co-ordinated Infrastructure Network (NNCI) under Award Number ECCS-1542202.

Abstract

Introduction and Objectives. The objective of this work is to enhance the *"fundamental knowledge base"* of the "*generation, stabilization and worsening*" shipboard oil/water emulsions in the presence of complex, yet tunable, hydrodynamic fields with varied chemical conditions (quotes from SERDP Statement of Need, SON). The separation of emulsified oil from bilge waters poses a unique challenge due to the inherent complexity and stability of these oil/water emulsion systems. Comprehensive scientific analysis of shipboard emulsions is needed to facilitate appropriate water treatment necessary for proper disposal. It is hypothesized here that by studying the oil-in-water system on length and time scales relevant to shipboard chemical composition and treatment processes, new insights into dynamics of shipboard emulsions is possible, which will ultimately aid in developing more efficient processing techniques for their separation.

Technical Approach. This work uses two complementary approaches to study single-droplet (Task 1, Microfluidic flows) and bulk (Task 2, Taylor-Couette, TC, flows) emulsion dynamics at the micro- and macro-scale, respectively. Many of the factors are explored, including "*shear/mixing, salinity, interfacial tension, and water/oil/surfactant ratios*". For Task 1, droplet microfluidic platforms are used as a high-throughput method to measure dynamic interfacial tension and quantify coalescence dynamics based on critical parameters such as surfactant type and concentration. This task will yield fundamental knowledge about the effect of additives present in bilgewater on the generation and stability of these complex emulsions. For Task 2, the experimental set-up will include injecting the dispersed phase into the continuous phase during flow using TC flow cell. Changes in droplet size distributions under varied flow types and turbulence intensities will be measured. Ultimately, insight will be gained into the kinetic processes involved in the emulsification process in tunable hydrodynamic fields.

Results. In Task 1, optimized design of microfluidic devices for dynamic IFT measurement and droplet coalescence experiments were successfully reached using surface treatment to yield hydrophilic walls suitable for oil-in-water systems. Dynamic IFT measurement of simulated bilgewater with detergent mix and model surfactants for oil-in-water systems has proven to result in different time-dependent profiles than those obtained in water-in-oil systems, suggesting a curvature dependent surfactant transport mechanism. The characterization of surfactant parameters using different isotherm models reveals the fundamental properties of both model and commercial surfactants in bilgewater system. Finally, the preliminary results of Stokes' trap experiments have shown successful trap and coalescence of droplets in water-in-oil systems. In Task 2, static emulsion stability tests found the non-monotonic relations for emulsion destabilization times with both oil and surfactant concentration. For oil contents greater than 10% oil, flow-induced destabilization was observed in rheometric shear flows. Similar flow-induc'sed destabilization was observed for lower oil contents, down to 0.1% oil, when exposed to more complex TC flows. The changes in stability were determined through changes in droplet size distributions. Finally, the preliminary results with in-situ injection in TC flows enables further advanced studies of the dynamics of emulsion formation and destabilization in flow.

Benefits. The results from Task 1 provide a new understanding of the effects of water/oil/surfactant ratios on time-dependent properties that impact emulsion formation, stability, and worsening. The results from Task 2 provide a new understanding of hydrodynamic effects on the transient emulsification and destabilization processes. Ultimately, the results of this project can inform the Department of Defense treatment strategies and will "*assist the development of methodologies or technologies that can mitigate the formation and undesired consequences of shipboard emulsions*", through improved understanding of the factors that govern emulsions.

Executive Summary

Introduction

The shipboard bilgewater is a complex wastewater found in the bottom chamber of ships, which is composed of sea water, fuels, oil, grease, detergents, and other pollutants [1, 2, 3]. In order to prevent the pollution caused by the discharge of bilgewater, the International Maritime Organization (IMO) has prohibited the direct offshore discharge of the bilgewater into seas and oceans with more than 15 mg L^{-1} oil that will be extremely harmful to the environment [4, 5, 6]. In this scenario, to comply with this environmental regulation, the Oil Pollution Abatement (OPA) systems are employed for managing shipboard waste [1]. The OPA systems have the equipment to collect, hold, treat, and analyze those oily waste on board, especially the bilgewater. It is required to remove the oil from the bilgewater with onboard treatment prior to discharge. Due to the presence of the surfactants in the detergents. However, the oily wastewater emulsions formed in the bilgewater are chemically stabilized, which makes them difficult to treat through primary gravity-based separation processes alone. The surfactant molecules, with hydrophobic tail and hydrophilic head, are attracted to the liquid-liquid interfaces, reducing the interfacial tension of the oil droplets in the water. This reduction of interfacial tension increases stabilization of the emulsion and limits coalescence of the dispersed phase droplets. Hence, in order to address the difficulty of removing those surfactant stabilized oil droplets from the emulsion and enhance the separation, fundamental understanding of the surfactant transport mechanism, and the effect of surfactant type, concentration, and oil/water ratio on the emulsion's stability is demanded.

Objectives

The main objective of this work is to enhance the "*fundamental knowledge base*" of the "*generation, stabilization and worsening*" (SON) shipboard oil/water emulsions in the presence of complex, yet tunable, hydrodynamic fields with varied factors. The separation of emulsified oil from bilge waters poses a unique challenge due to the inherent complexity and stability of these oil/water emulsions systems. Comprehensive scientific analysis of shipboard emulsions is needed to facilitate appropriate water treatment necessary for proper disposal. It is hypothesized here that by studying the oil-in-water system on length and time scales relevant to shipboard chemical composition and treatment processes, new insights into the dynamics of shipboard emulsions will be possible, ultimately aiding in the development of more efficient processing and separation techniques.

This work uses two complementary approaches to study single-droplet (Task 1, Microfluidic flows) and bulk (Task 2, Taylor-Couette, TC, flows) emulsion dynamics at the micro- and macro-scale, respectively. Many of the factors are explored, including "*shear/mixing, salinity, interfacial tension, and water/oil/surfactant ratios*" (SON). Task 1 answers the questions of the effects of water/oil/surfactant ratios on time- dependent material properties that impact emulsion formation, stability, and worsening. This task yields new knowledge on the effect of additives present in bilgewater on the stability of these complex emulsions. Task 2 answers the questions of hydrodynamic effects on transient emulsification processes to confirm flow states that either

enhance or reduce emulsion stability. Ultimately, insight can be gained into the kinetic processes involved in the emulsification process in tunable hydrodynamic fields.

Technical Approach

Task 1 - Microscale Droplet using Microfluidics. On the microscale, droplet microfluidic flows are used to generate and trap droplets in tunable chemical and flow conditions, to allow characterization of isolated single droplets within an emulsion. In this task, the effect of oil/water/surfactant ratios on emulsion generation, properties, and stability is studied using droplet microfluidics, by performing surface treatments on microfluidic devices (Objective 1), measurements of dynamic interfacial tension (Objective 2), characterization of surfactant transport (Objective 3), and investigation of the droplet coalescence and film drainage (Objective 4).

Objective 1 Deliverable. The surface treatment protocol for performing measurements of simulated bilgewater systems is established. The bonded PDMS (polydimethylsiloxane) devices are exposed to a secondary oxygen plasma treatment with *150 W* for *15 minutes* subject to oxygen flow at *300 sccm*, and then immediately stored in DI water under vacuum for at least 7 days. Performance tests on the treated device show that diesel oil mix droplets are successfully generated in continuous synthetic sea water (SSW) phase and the device remains hydrophilic for over 4 hours, which provides the sufficient time for running one dynamic IFT experiment.

Objective 2 Deliverable. The dynamic interfacial tension of droplets in simulated water-in-oil (w:o) and oil-in-water (o:w) bilgewater is measured using a microfluidic device as shown in **Figure E1**, using the treatment protocol from Objective 1 for the o:w systems. Oil droplets ("Dispersive" phase) are formed in an outer phase (both the "Sheath" and "Continuous" phase) of water using a T-junction formation mechanism, and then transported to a series of microfluidic interfacial tensiometers. The recorded droplet deformations are analyzed through edge detection, and the IFT is obtained from theoretical equations.

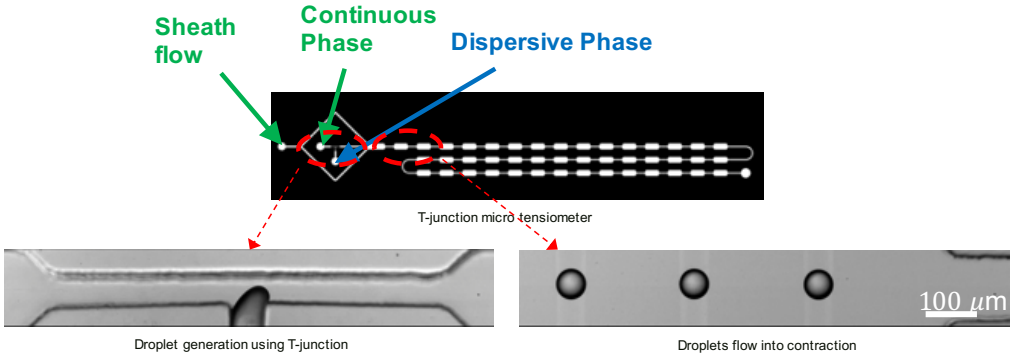

Figure E1. T-junction microfluidics device for dynamic IFT measurement. Droplets are generated at the T-junction and travel with the continuous phase to the downstream contraction, where the IFT measurements are made. The distance between the droplets are controlled by the sheath flow.

Objective 3 Deliverable. The IFT measured is used to extract the parameters of the surfactant using isotherm models including Langmuir and Frumkin models for the chemical systems explored

in Objective 2. The maximum surface coverage, adsorption constant, surfactant diffusivity, and adsorption/desorption rate constant are calculated for both o:w and w:o systems.

Objective 4 Deliverable. Droplet coalescence experiments are performed using a microfluidic Stokes-trap device as shown in **Figure E2**. Droplets are generated upstream and later trapped downstream in the cross-slot region of the device. By adjusting the pressure to each channel, a droplet is held inside the trapping region, while new droplets are allowed to collide and coalescence with the trapped droplet. The film drainage time between the two droplets is extracted from the recorded video for model bilgewater systems.

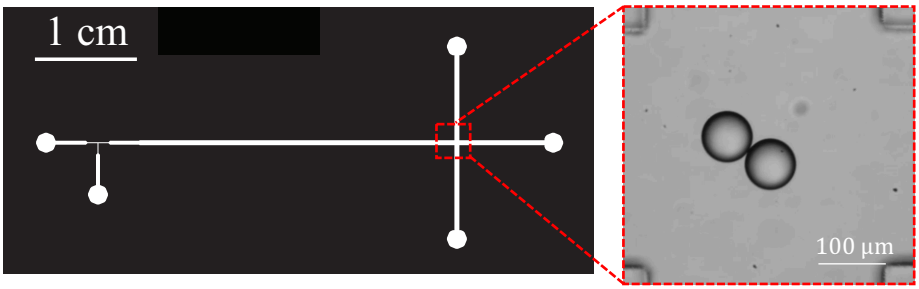

Figure E2. (Left) Microfluidics Stokes' trap device (Right) Two trapped droplets interacting at the stagnation point of the cross-slot of a microfluidics Stokes-trap device.

Task 2 - Macroscale Taylor-Couette Flows. On the macroscale, Taylor-Couette (TC) flow, or flow between concentric rotating cylinders, is used to study age and mixing conditions on emulsion generation and stability. The effect of oil/water/surfactant ratios and flow conditions on emulsion formation and stability is studied, by performing static emulsion stability tests (Objective 1), steady shear viscosity measurements (Objective 2), studies on the hydrodynamic effects on *pre-prepared* simulated bilgewater emulsion stability under different kinematic TC flow types and turbulent intensities (Objective 3), and *in-situ* emulsion formation and stability study under different kinematic TC flow types and turbulent intensities (Objective 4).

Objective 1 Deliverable. The droplet stability is determined for each system via the measurement of emulsion turbidity in a centrifuge tube, as shown in **Figure E3**. Transparent vials containing the sample are observed over a period of days using a camera and image analysis. The change in the opaqueness (turbidity) of the sample is used to determine the destabilization time for a variety of simulated bilgewater and model systems.

Objective 2 Deliverable. Viscosity of the emulsion as of a function of shear rate is determined using a rotational rheometer for the simulated bilgewater and model systems. This viscosity is needed to calculate the dimensionless cylinder speed (Reynolds number), based on the global shear rate. It also serves as a metric for emulsion stability under shear. Systems with hysteretic, or history-dependent, viscosity profiles inducted macroscale phase separation. Results of emulsion destabilization are supported with droplet size distribution measurements. Systems with 10% oil and higher experienced flow-induced stabilization in the rheometric cup-and-bob geometry up to an apparent shear rate of 4000 s^{-1}, while systems with lower oil content showed no change.

Objective 3 Deliverable. Pre-prepared simulated and model bilgewater emulsions are studied into the TC cell, shown in **Figure E4**. Different flow conditions, such as laminar wavy vortex, turbulent

wavy vortex, turbulent Taylor vortex are tested to study the stability of bilgewater emulsions and evolution of emulsion droplet size distribution. Unlike in Objective 2, the systems with oil content as low at 0.1% oil demonstrated flow-induced destabilization when exposed to the TC turbulent flow states.

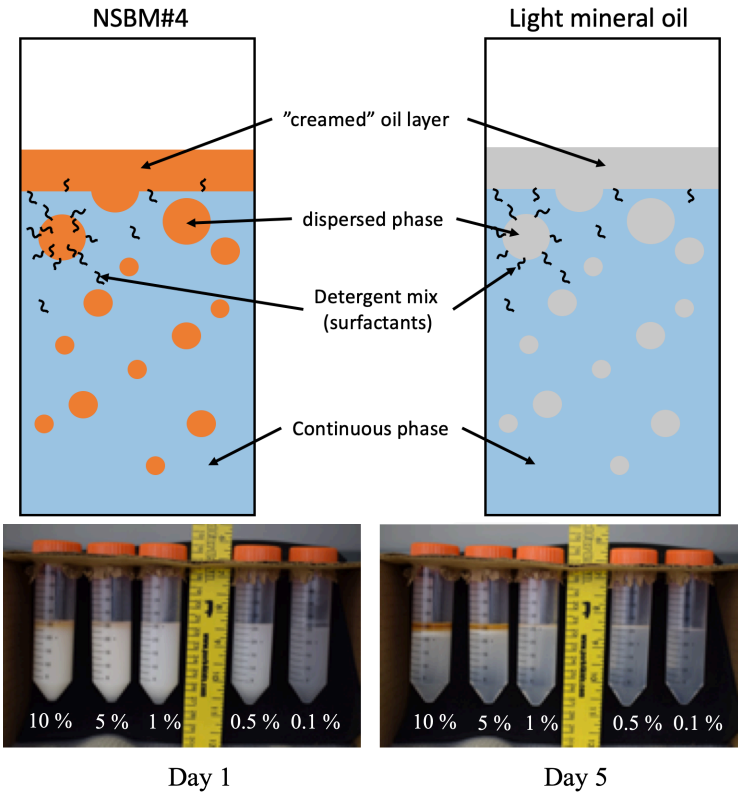

Figure E3. Schematics of the static stability test. Two different systems are tested: Navy Simulated Bilgewater Mixture (NSBM#4) in water (Top left) and LMO in water (Top right). Detergent mix is added to the water phase for both systems. (Bottom) Stability test shows phase separation due to destabilization of the emulsion. The o:w ratio of the samples (from left to right) are 10%, 5%, 1%, 0.5%, and 0.1%. Each contain 10 ppm of the SERDP detergent mix.

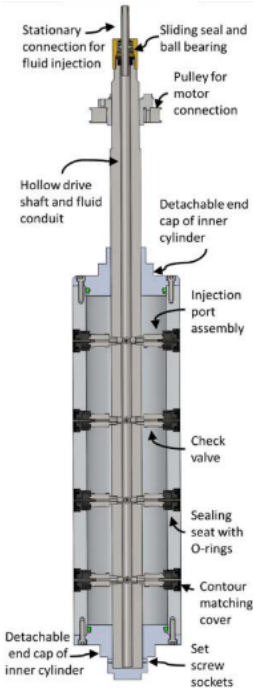

Figure. E4 Schematic of the TC inner cylinder showing the injection system

Objective 4 Deliverable. In-situ emulsion formulation and destabilization experiments were conducted in the same TC cell as Objective 3, where oil or emulsified oil is directly injected into the annulus containing only surfactant-laden water at high mixing speed. The flow conditions in the cell is also subject to the same different flow type as in Deliverable 3, and the changes in the size distribution of the emulsions are determined.

Results and Discussion

Task 1, Objective 1: Surface Treatment of Microfluidic Devices. The hydrophilic treatment method has been optimized for best surface treatment for our device: The bonded PDMS device is exposed to a second oxygen plasma treatment with *150 W* for *15 minutes* subject to oxygen flow at *300 sccm*. After the treatment, the device is immediately stored in DI water under vacuum at least for 7 days. The treated device is then tested and the result shows that diesel oil mix droplets are successfully generated in continuous SSW phase and the device remains hydrophilic for over 4 hours, which provides the sufficient time for running one dynamic IFT experiment. In addition, the wettability of the device has been significantly improved with no droplets attached on the channel wall.

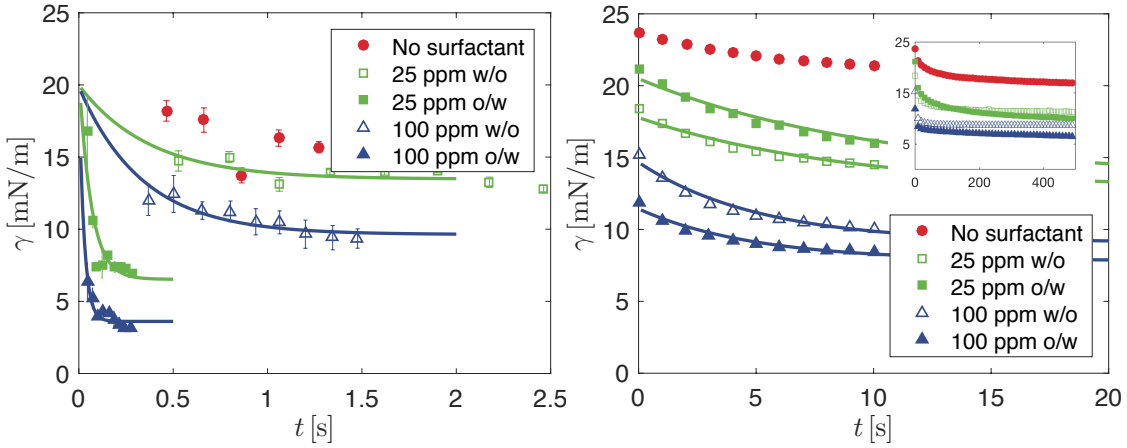

Figure E5. Dynamic IFT (γ) of droplets as a function of time (t) with no surfactant, 25 ppm and 100 ppm detergent mix for water-in-oil and oil-in-water using (left) microfluidic tensiometry and (right) pendant drop measurements. The inset figure shows the IFT of a pendant drop over long-time scale. The time scale for the decay in IFT for each experiment is extracted by fitting the $\gamma - t$ curve with the exponential function, $\gamma = a\,exp(-t/\tau) + b$, shown as the solid lines in the plot.

Task 1, Objective 2: Dynamic IFT of Microscale Droplet using Microfluidics. When the surfactant is added at 25 ppm (below the critical micelle concentration, CMC) and 100 ppm (above CMC), there is clear decrease in equilibrium IFT as shown in **Figure E5**, which shows the effect on the IFT from the addition of surfactant. In most cases, the equilibrium IFT from microfluidics agrees with the measurement from pendant drop over long-time scale in the inset. However, the IFT drops significantly within 2 seconds for microfluidic droplets, while the IFT decays at order of 100 seconds from pendant drop measurements. Given the fact that the diameter of droplets is about 75 μm in microfluidics and 2 mm for pendant drop, the rate of decay of dynamic IFT is apparently dependent on the size. the IFT decays even faster (within 1 second) for oil-in-water o:w compared to water-in-oil w:o (within 2 seconds) for micro-scale droplets as shown in **Figure E5** (left), which indicates a phase dependency of the surfactant transport. On the contrary, the rate of decay does not change significantly for pendant drop IFT when the surfactant is added to the outer phase in **Figure E5** (right).

Task 1, Objective 3: Characterization of Surfactant. The extracted values of the maximum surface coverage Γ_∞ for both surfactants are in the reasonable order of magnitude for surfactant molecules, while the diffusivity $D_{C<CMC}$ of the simulated detergent mix is one order of magnitude smaller than the typical value ($10^{-10}\ m^2/s$). On the other hand, a higher value of the Langmuir coefficient κ is obtained for the model surfactant AES than that for the simulated detergent mix, suggesting that the surfactant molecule of AES is more active than that of detergent mix. The calculated adsorption rate is smaller when the surfactant is inside the droplet, suggesting a larger energy barrier for the surfactant molecules. For these systems, NSBM#4 is used for the oil phase and SSW for the water phase. In this objective, additional model systems of light mineral oil LMO and distilled water, with the model surfactants, TritonX-100 and SDS, and commercial surfactants found on board Navy vessels, Type 1, Solid Surge, and PRC, are studied. The calculated data of κ

are also compared to that of other commonly used surfactants as shown in **Figure E6.** Particularly, κ of Type 1, TritonX-100, PRC and Solid Surge are relatively higher than that of other surfactants.

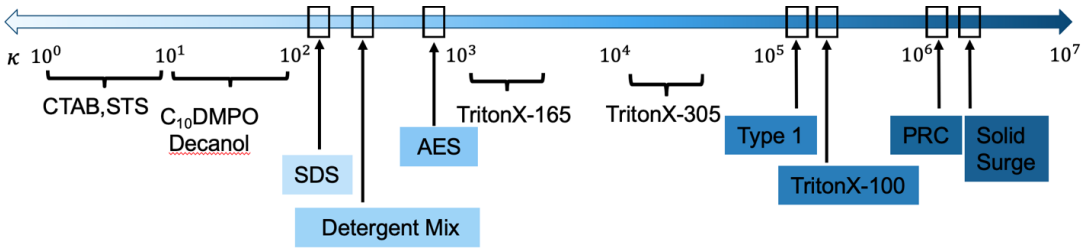

Figure E6. Comparison of κ for the calculated surfactants with other commonly used surfactants. The larger the κ, the more the surfactant tends to reduce the IFT.

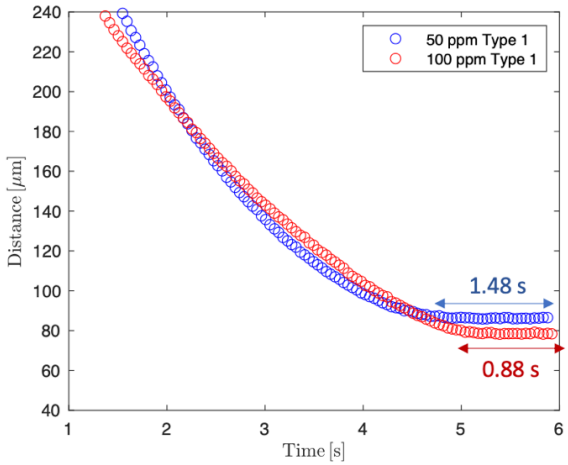

Figure E7. Film drainage time of droplet coalescence for distilled water in LMO with 50 ppm and 100 ppm commercial surfactant Type 1 in water. Both show the film drainage time of around 1 second.

Task 1, Objective 4: Droplet Coalescence and Film Drainage Time. Preliminary tests of droplet trapping and coalescence has been performed for mineral oil droplets in water using a 4-channel Stokes' trap device. Three systems were used for those experiments. 1) Distilled water in NSBM#4 with detergent mix surfactant; and distilled water in light mineral oil with 2) detergent mix and 3) Type 1 commercial surfactant. For the third system, 50 ppm and 100 ppm Type 1 were used, and the film drainage time is shown as **Figure E7.** It took about ~0.88 s for 100 ppm and ~1.48s for 50 ppm.

Task 2, Objective 1: Static Bulk emulsion Stability Test. The timescales associated with the destabilization time are extracted using an exponential function fitted to the time-dependent turbidity plot based on the processed images from the centrifuge tube tests. The time constant versus o:w ratio as shown in **Figure E8** reveals a general non-monotonic trend with a peak in stability around 5% for NSBM#4, while there is a surfactant concentration dependent peak location for mineral oil. The peak location of the time constant that is fixed at around 5% o:w for NSBM#4 cases were explained due to the already existing surfactants soluble in the complex NSBM#4,

which also stabilizes the interface. The time constant was also determined as a function of the surfactant concentration at various o:w ratios, and was also found to be non-monotonic.

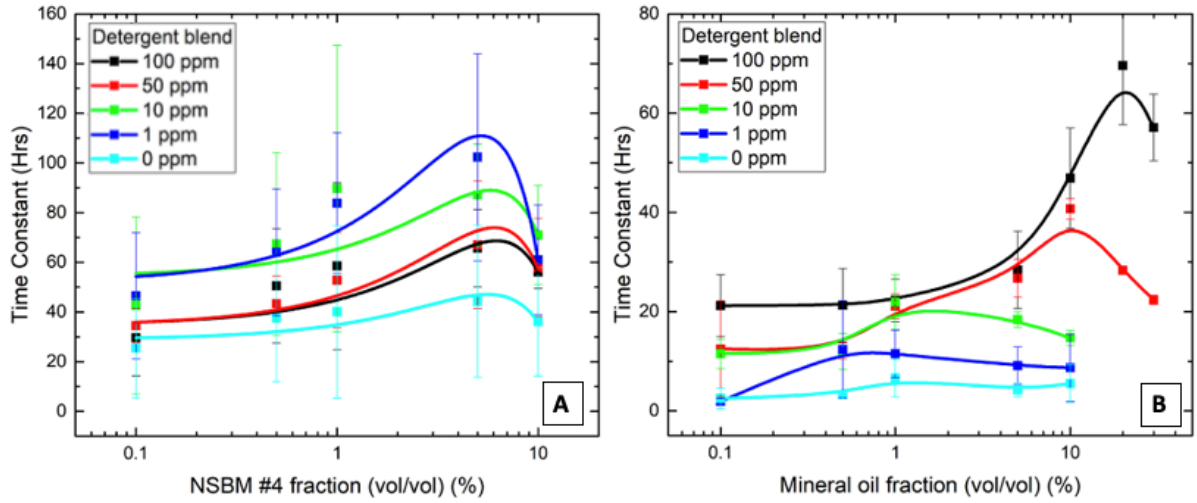

Figure E8. (A) Plots of exponential decay time constant for the NSBM#4 system, varying with oil fraction. Low values of the time constant correspond to a rapidly destabilizing system, while high values of the time constant correspond to slow destabilization. The plots show the trend of increasing stability with oil fraction until 10% oil is reached. The curves here are quadratic best fits. (B) Plots of exponential decay time constant for the light mineral oil system, varying with oil fraction, showing the trend of increasing stability with oil fraction, a peak is reached. The peak location is dependent on surfactant concentration.

Task 2, Objective 2: Simple-shear Bulk Emulsion Viscosity Measurement. Rheometry was performed on simulated bilge emulsion samples of 0.1%, 0.5%, 1%, 5%, and 10% oil in water (o:w) ratios at 100, 50, and 10 ppm of SERDP surfactant blend and 100 ppm LAS model surfactant, as well as 10% o:w at 1 ppm surfactant. **Figure E9** shows a representative example of the expected behavior, for 0.5% oil with 10 ppm detergent mix. For all samples with 10% o:w ratios oil or below, the viscosity plateaus at a value slightly above that of water, and independent of shear rate (exhibiting Newtonian-like behavior). The front sweeps (low-to-high shear rate) and back sweeps (high to low shear rates) for all of these samples yielded the same results. However, for all samples with 10% oil or above, a hysteresis effect was observed. It is suspected that this is because of destabilization of high o:w emulsions, leading to increased creaming of the oil phase and a macroscale change in phase state.

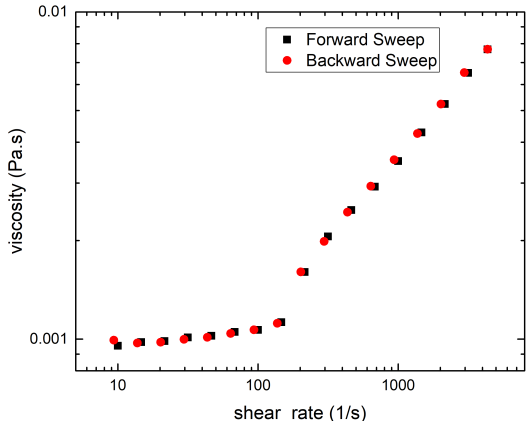

Figure E9. Steady-shear viscosity of 0.5 % NSBM#4 oil with 10 ppm detergent mix, as a function of shear rate. In general, regions of constant viscosity are observed for low to moderate shear rates, depending on the sample. The appearance of shear thickening (increase in viscosity with shear rate) at high shear rates is due to flow instabilities and are an artifact of the measurement. Chemical compositions with 10% oil or greater show a hysteresis behavior, due to emulsion destabilization.

Task 2, Objective 3: Pre-prepared Emulsion Stability Test in TC Flows. Experiments were performed on large volumes of 0.1% o:w, 100 ppm surfactant simulated bilge emulsion using a custom-built Taylor-Couette Cell, with representative results shown in **Figure E10**. A decrease in droplets of a size less than 10 micrometers and a corresponding increase in droplets of size on the order of 100 microns occurred with time, likely due to emulsion destabilization – similar to that observed in traditional vial tests. This destabilization effect was more pronounced in a sample that underwent the "ramp" Taylor-Couette test, due to enhanced destabilization from the flow. Similar shifts in size distributions were not observed in 0.1% o:w samples with rheometry alone (Objective 2), and are suggestive of the importance of the flow and mixing types in emulsion destabilization and can be used to inform conditions for liquid-liquid separation technologies. Identical experiments to the first type laid out above were also performed on emulsion systems with variations in ingredients, in order to gauge the effect changes to the emulsion system would have on the behavior of droplet size distributions in Taylor-Couette flow.

Task 2, Objective 4: In-situ Emulsion Formation and Stability in TC Flows. Several proof of concept experiments were performed as a function of solution composition and mixing speeds, to optimize the in-situ TC experiments. Results showed that there was some degree of emulsification at highest shear rates (mixing speed) but as soon as the mixing speed was reduced, the oil droplets in the solution destabilized and separated out from the solution. The results also showed that higher oil concentration, higher surfactant concentration, and Type 1 surfactant yielded the most stable emulsions in the TC cell. The formation of smaller droplet sizes is initially observed, followed by the formation of larger droplets (likely due to coalescence) with higher mixing speeds.

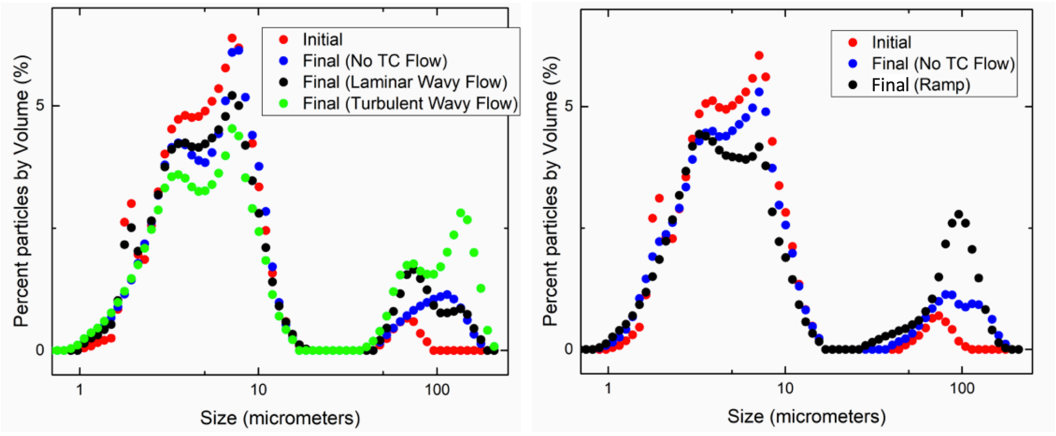

Figure E10. Pre-prepared emulsion of 0.1% NSBM#4 oil in water with 100 ppm detergent mix tested in Taylor-Couette cell for (left) "step-wise" and (right) "ramped" flow condition. Both show a decrease in the number of droplets of size less than 10 micrometers and a corresponding increase in droplets of size on the order of 100 microns with time, due to emulsion destabilization.

Implications for Future Research and Benefits

Future Research. Both tasks end with proof of concept experiments that set the stage for advance studies of emulsion stability. For example, the preliminary results of the Stokes' Trap experiments have shown the successful trapping and coalescence of the droplets for bilgewater systems. Future work includes systematic coalescence studies in a 6-channel trap (with two droplets trapped simultaneously) for study of the stability of both bilgewater and fire-fighting foam surfactant-laden systems. In these studies, different surfactants with various concentrations will be used, and film drainage times during coalescence and coarsening will be determined. In addition, the in-situ formation and emulsion stability in TC flow enables us to observe the formation of emulsions at much lower shear rates and provides a framework for further exploration to study mixing dynamics of oil-water emulsions in different TC flow conditions. In these experiments, the dynamic mixing of concentrated emulsions into the water-surfactant solution was successfully visualized in different flow conditions, allowing for future mass transfer studies and determination of dispersion coefficients for these complex emulsions.

Benefits. The results from micro-scale droplet studies in Task 1 provide fundamental new understanding of the droplet size and phase dependence of surfactant on dynamic IFT and droplet coalescence. These results further provide insight into time-dependent surfactant transport properties that impact emulsion formation, stability, and worsening. The results from macro-scale bulk emulsion study in TC cell provide a new understanding of the hydrodynamic effects on the transient emulsification process to confirm flow states that either enhance or reduce emulsion stability. Ultimately, the results of this project are of significance for the Department of Defense for enhanced treatment strategies of the oily bilgewater systems and will "*assist the development of methodologies or technologies that can mitigate the formation and undesired consequences of shipboard emulsions*" (SON), through an improved understanding of the factors that govern emulsions.

Full Report

Objectives

The main objective of this work is to enhance the "*fundamental knowledge base*" of the "*generation, stabilization and worsening*" (SON) shipboard oil/water emulsions in the presence of complex, yet tunable, hydrodynamic fields with varied factors. The separation of emulsified oil from bilge waters poses a unique challenge due to the inherent complexity and stability of these oil/water emulsions systems. Comprehensive scientific analysis of shipboard emulsions is needed to facilitate appropriate water treatment necessary for proper disposal. It is hypothesized here that by studying the oil-in-water system on length and time scales relevant to shipboard chemical composition and treatment processes, new insights into dynamics of shipboard emulsions will be possible, ultimately aiding in the development of more efficient processing and separation techniques.

This work uses two complementary approaches to study single-droplet (Task 1, Microfluidic flows) and bulk (Task 2, Taylor-Couette, TC, flows) emulsion dynamics at the micro- and macro-scale, respectively. Many of the factors are explored, including "*shear/mixing, salinity, interfacial tension, and water/oil/surfactant ratios*" (SON). Task 1 answers the questions of the effects of water/oil/surfactant ratios on time- dependent material properties that impact emulsion formation, stability, and worsening. This task yields new knowledge on the effect of additives present in bilgewater on the stability of these complex emulsions. Task 2 answers the questions of hydrodynamic effects on transient emulsification processes to confirm flow states that either enhance or reduce emulsion stability. Ultimately, insight can be gained into the kinetic processes involved in the emulsification process in tunable hydrodynamic fields.

Task 1 - Microscale Droplet using Microfluidics

On the microscale, droplet microfluidic flows are used to generate, and trap droplets in tunable chemical and flow conditions. This will allow characterization of isolated single droplets within an emulsion. In this task, the effect of oil/water/surfactant ratios on emulsion generation, properties, and stability is studied using droplet microfluidics, by performing surface treatments on microfluidic devices (Objective 1), measurements of dynamic interfacial tension (Objective 2), characterization of surfactant transport (Objective 3) and by investigating the droplet coalescence and film drainage (Objective 4). These four objectives, resulting in 4 deliverables, are detailed here:

Objective 1 Deliverable: Microfluidic devices surface treatment. The devices used in the current study are based on the PDMS, which is a hydrophobic material. However, the systems studied for bilgewater contain water in the continuous phase and oil in the dispersive phase, which requires the channel wall to be hydrophilic. Thus, the surface treatment for the PDMS based microfluidic devices is needed. The goal of this deliverable is to investigate various treatment methods and find optimal procedures for the hydrophilic treatment. *The desired outcome of this deliverable* is, after the treatment, to successfully generate droplets, measure the droplet deformation and trap the

droplets for oil-in-water systems. This deliverable is to assist the performance of the experiments for Task 1, Deliverables 2 and 4.

Objective 2 Deliverable: Dynamic interfacial tension (IFT) measurements of bilgewater with a microfluidic tensiometer. The goal is to investigate the fundamental mechanisms that govern surfactant transport to the oil-water interface in bilgewater emulsions, including diffusion as well as adsorption and desorption, at varied oil/water/surfactant ratios. Time dependent IFT on microscale drops can provide insights into the transport mechanisms governing the dynamic behavior of these interfaces. The desired outcome of this deliverable is to collect IFT measurements at varied surfactant concentrations relative to the critical micelle concentration (CMC), which informs the amount of detergent which results in the creation and stabilization of bilgewater emulsions. This deliverable also informs which systems would be best for study in Task 1, Deliverables 2 and 3.

Objective 3 Deliverable: Characterization of Surfactant Transport. In addition to providing interfacial tension as a function of time with certain surfactants, the measured IFT from Task 1 Deliverable 2 also gives insight into key properties of the surfactants, such as the diffusivity, interface coverage, and adsorption rate of the surfactant molecules, which can be extracted from dynamic IFT data using appropriate surfactant transport models. These properties imply the transport behavior of the surfactant molecules, such as the time scale and the tendency to adsorb onto the interface. *The desired outcome of this deliverable* is to calculate the properties of the surfactants based on the IFT in Task 1 Deliverable 2 using different isotherm and transport models. This deliverable also informs which system would be best for the study in Task 1, Deliverable 4.

Objective 4 Deliverable: Coalescence estimates with 4-channel and 6-channel cross-slot Stokes trap. The 6-channel cross-slot creates two stagnations points and thus can simultaneously trap two droplets. *The desired outcome for this deliverable* is proof of concept that this design can produce quantitative measurements of droplet coalescence probability and film drainage time as a function of viscosity ratio, and surfactant concentration. Quantifying the various parameters affecting droplet coalescence and consequently emulsion stability on a microscale will aid in improvement of process control to enhance the efficiency for oil-water separation in shipboard emulsions.

Task 2 - Macroscale Taylor-Couette Flows

On the macroscale, Taylor-Couette (TC) flow, or flow between concentric rotating cylinders, is used to study age and mixing conditions on emulsion generation and stability. The effect of oil/water/surfactant ratios and flow conditions on emulsion formation and stability is studied, by performing static emulsion stability tests (Objective 1), steady shear viscosity measurements (Objective 2), hydrodynamic effects on *pre-prepared* simulated bilgewater emulsion stability under different kinematic TC flow types and turbulent intensities (Objective 3), *in-situ* emulsion formation and stability study under different kinematic TC flow types and turbulent intensities (Objective 4).

Objective 1 Deliverable: Static emulsion stability test. Bulk emulsion stability tests are performed with long timescale without external flow conditions. *The desired outcome of this study is* to understand the dependence of stability on oil volume fraction and surfactant concentration for bulk

emulsions. Particularly, the test are performed in centrifuge vials, and the turbidity of the emulsion and droplet size distributions are investigated.

Objective 2 Deliverable: Steady-shear emulsion viscosity measurement. Viscosity of the bulk emulsion are measured based on various oil volume fraction and surfactant concentration through the rheometer under simple shear. *The desired outcome of this study* is to understand the viscosity change of the emulsion, which also is determined by the droplet size distribution and stability in the bulk. The results here will also provide insight into the emulsion stability under shear stress.

Objective 3 Deliverable: Hydrodynamic effects on pre-prepared simulated bilgewater emulsion stability under different kinematic flow types and turbulent intensities. The goal of this deliverable is to study the effect of shear under different kinematic flow types (vortex structure) on the stability of pre-prepared emulsions. The desired outcome of deliverable 1 is to have a specific hydrodynamic processing protocol to decrease emulsion stability to aid in shipboard separations. Our current TC cell [7, 8, 9] (see **Figure 8**) offers the possibility of continuous axial flow and thus the ability to study residence time requirements for continuous processing of emulsions, rather than limited to batch processing. The modified TC cell used here includes radial injection ports, to inject the dispersed phase directly into the flow field and study emulsion formation and stability in flow. The results of this deliverable are discussed in detail in this report. Flow fields, such as Taylor Vortex Flow are established by setting the angular velocity of the inner cylinder.

Objective 4 Deliverable: In-situ emulsion formation and stability study under different kinematic flow types and turbulent intensities. The goal of this deliverable is to study the effect of different kinematic flow types (vortex structure) on the in-situ formation of emulsions. Systems characterized in Task Deliverable 1 will be candidates for study here. *The desired outcome* of Deliverable 4 is the determination of specific hydrodynamic features that create stable emulsions, to provide recommendations for shipboard storage and treatment.

Background

Inevitable contamination of shipboard water in a vessel's bilge produces liquid-liquid emulsions. These complex emulsions are generated both chemically and mechanically and consist of mixtures of oils, fuel, detergents and surfactants, lubricants heavy metals, different charged species and other trace elements suspended in water. [10] Any water containing more than 15 parts per million (ppm) of oil, such as bilgewater, cannot be discharged overboard (MARPOL Annex 1), [11] and must be stored or treated. Comprehensive analysis of shipboard emulsions is needed to facilitate appropriate water treatment necessary for proper disposal. The presence of surface-active species and surface charge often contributes to the formation of thermodynamically stable oil in water emulsions. These shipboard emulsions typically contain oil in both the free phase and dispersed phase. [12] The oil droplets in the free phase are often larger in size than the typical colloidal range (50 micron) and coalesce naturally at longer times to form a floating thin film on top of the aqueous phase. Oil drops in the dispersed phase, which are smaller than 50 microns, possess greater thermodynamic resistance to coalescence and thus need more sophisticated methods than gravitational separation for effective removal.

Emulsion stability largely depends on the droplet size distribution, which is further affected by interfacial tension, hydrodynamic forces, concentration/composition of emulsifier(s), presence of solid particulates, and the bulk properties of the oil and water phases. [13, 14, 15] Upon emulsion formation, there are a variety of processes that can occur to break down the emulsion. Some of these processes include creaming and sedimentation, flocculation, Ostwald ripening, coalescence, and phase inversion. [15] Many processes can occur simultaneously within a complex emulsion system, and the underlying physical phenomena behind these processes are complex. [15, 16] Theoretical treatments of macroscale emulsion stability are nontrivial because monodisperse droplets are difficult to produce without employing microfluidic channels, therefore bulk emulsion stability models are semi-empirical at best. [15, 17, 18] Despite these challenges, droplet size distribution and emulsion stability toward creaming or sedimentation remain commonly used quantifiable indicators of emulsion stability. [19, 20, 21]

Materials and Methods

Technical Approach for Task 1, Objective 1: The microfluidic channel is fabricated using PDMS based on the SU-8 mold on a silicon wafer. However, as the PDMS material is a hydrophobic material, hydrophilic treatment on PDMS was required to invert the liquid phases, to more closely represent oil-in-water bilge emulsions. The method of treatment is modified from the work by Tan et al. [22] and has been optimized for best surface treatment for our device: The bonded PDMS devices are exposed to a secondary oxygen plasma treatment with *150 W* for *15 minutes* subject to oxygen flow at *300 sccm*, and then immediately stored in DI water under vacuum for at least 7 days. Performance tests on the treated device show that diesel oil mix droplets are successfully generated in continuous synthetic sea water (SSW) phase and the device remains hydrophilic for over 4 hours, which provides the sufficient time for running one dynamic IFT experiment. The parameters used for the plasma treatment has been optimized for different geometries of the microfluidic devices.

Technical Approach for Task 1, Objective 2: The dynamic interfacial tension of droplets in simulated water-in-oil (w:o) and oil-in-water (o:w) bilgewater is measured using a microfluidic device as shown in **Figure 1,** using the treatment protocol from Objective 1 for the o:w systems. Oil droplets ("Dispersive" phase) are formed in an outer phase (both the "Sheath" and "Continuous" phase) of water using a T-junction formation mechanism, and then transported to a series of microfluidic interfacial tensiometers based on the design by Hudson and co-workers. [23] As the droplet passes through the sudden change in geometry, it undergoes a deformation from a spherical shape to an elongated ellipse (see **Figure 2**). The degree of deformation is determined by the extensional strain acting on the droplet by the flow (a deforming force) and the droplet interfacial tension (a restoring force). Furthermore, due to the serpentine geometry of the channel, high-speed videos of deforming droplets can be recorded at several tensiometers located along the length of the device, to examine the kinetics of transport of surface-active species introduced into the dispersed phase inlet. In these IFT experiments, the viscosities of the two phases, extensional strain rate, droplet velocity, size and deformation (quantified by a dimensionless deformation parameter), are known or measured using a camera at up to 40,000 frames per second and provided as inputs to a custom-built image-processing code implemented using MATLAB. Therefore, all other terms of a droplet stress balance equation are known or calculated directly from measurements, enabling

calculations of the dynamic interfacial tension of each droplet. Apart from the microfluidics experiments, the dynamic IFT of a millimeter-size droplet are also measured by the pendant drop method using KRUSS DSA 30 for all the conditions in microfluidics.

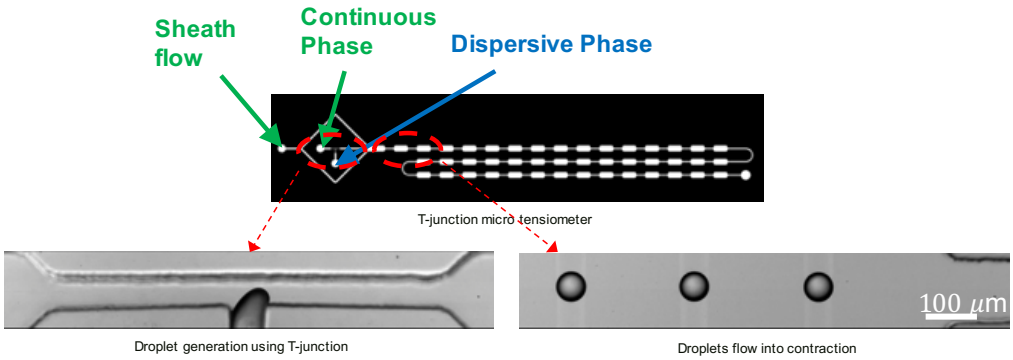

Figure 1. T-junction microfluidics device for dynamic IFT measurement. Droplets are generated at the T-junction and travel with the continuous phase to the downstream contraction, where the IFT measurements are made. The distance between the droplets are controlled by the sheath flow.

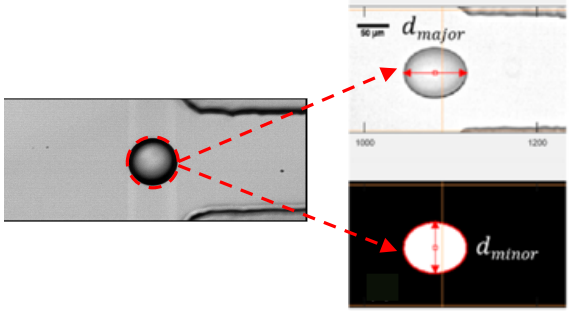

Figure 2. Droplets entering the contraction will experience deformation due to the flow field. The edge of deformed droplet is detected by MATLAB, enabling measurements of IFT for each droplet.

Simulated bilgewater is used following the SERDP recommendation for preparing the oil and detergent mix, with composition shown in **Table 1**. The synthetic sea water (SSW) is used as the water phase of the bilgewater emulsion in the current experiments. In addition to the detergent mix, model surfactant Alcohol Ethoxy Sulfate (AES) is also used as a comparison to detergent mix.

Table 1. SERDP Recommended Chemical Mixtures for Simulated Bilgewaters

1,000-ppm (vol/vol) Oil Mix ("NSBM#4")	**100-ppm (vol/vol) Detergent Mix**
50% - Diesel Fuel Marine (MIL-PRF-16884N)	50% - Type 1 General Purpose Detergent (MIL-D-16791G(1))
25% - 2190 TEP Steam Lube Oil (MIL-PRF-17331K)	25% - Commercial Detergent Tide Ultra (liquid)
25% - 9250 Diesel Lube Oil (MIL-PRF-9000L)	25% - Degreasing Solvent (MIL-PRF-680C, Type III)

A complete list of chemical systems studied in Deliverable 1 is given below in **Table 2** (next page), for both pendant drop and microfluidic ("μfluidic") methods, where the oil phase varies between

the NSBM#4 oil mix and light mineral oil (LMO), a salt-containing water phase is label SSW for synthetic sea water, and the Detergent Mix from **Table 1** is labeled "SERDP" under surfactant.

Table 2. Chemical Composition of Emulsions Studied in Task 1, Deliverable 1

Method	Oil Phase	Water Phase	Surfactant	Surfactant Concentration (ppm v/v)	Surf. Phase	~ Drop Size
Pendant Drop: Water in Oil	NSBM#4	SSW	SERDP	20, 25, 30, 35, 40, 50, 75, 100	Water	2 mm
	NSBM#4	SSW	SERDP	100	Oil	2 mm
	NSBM#4	SSW	LAS	100	Oil	2 mm
	NSBM#4	SSW	LAS	100	Water	2 mm
	NSBM#4	SSW	AES	100	Oil	2 mm
	NSBM#4	SSW	AES	100	Water	2 mm
	LMO	Water	LAS	100	Water	2 mm
	LMO	Water	LAS	100	Oil	2 mm
	LMO	Water	AES	100	Water	2 mm
	LMO	Water	AES	100	Oil	2 mm
Pendant Drop: Oil in Water	NSBM#4	SSW	SERDP	25, 100	Water	2mm
	NSBM#4	SSW	LAS	100	Water	2mm
	NSBM#4	SSW	AES	100	Water	2mm
	LMO	Water	LAS	100	Water	2mm
	LMO	Water	LAS	100	Oil	2mm
	LMO	Water	AES	100	Water	2mm
	LMO	Water	AES	100	Oil	2mm
	LMO	Water	TritonX-100	50, 100, 150, 300, 500, 600	Water	2mm
	LMO	Water	SDS	50, 100, 300, 500, 1000, 2000, 4000, 6000	Water	2mm
	LMO	Water	Type 1	50, 80, 100, 150, 300	Water	2mm
	LMO	Water	Solid Surge	100, 200, 300, 400, 500	Water	2mm
	LMO	Water	PRC	2000, 4000, 6000, 7000, 8000	Water	2mm
μfluidic: Water in Oil	NSBM#4	SSW	SERDP	25, 100	Water	80 μm
	NSBM#4	SSW	SERDP	100	Oil	80 μm
	NSBM#4	SSW	LAS	100	Water	80 μm
	NSBM#4	SSW	AES	100	Oil	80 μm
	NSBM#4	SSW	AES	10,100	Water	80 μm
	LMO	Water	LAS	100	Water	80 μm
	LMO	Water	LAS	100	Oil	80 μm
	LMO	Water	AES	100	Water	80 μm
	LMO	Water	AES	100	Oil	80 μm
μfluidic: Oil in Water	NSBM#4	SSW	SERDP	25, 100	Water	80 μm
	NSBM#4	SSW	LAS	100	Water	80 μm
	NSBM#4	SSW	AES	10,100	Water	80 μm
	LMO	Water	LAS	100	Water	80 μm
	LMO	Water	TritonX-100	50, 100, 150, 300, 500, 600	Water	80 μm
	LMO	Water	SDS	50, 100, 300, 500, 1000, 2000, 4000, 6000	Water	80 μm

	LMO	Water	Type 1	50, 80, 100, 150, 300	Water	80 μm
	LMO	Water	Solid Surge	100, 200, 300, 400, 500	Water	80 μm
	LMO	Water	PRC	2000, 4000, 6000, 7000, 8000	Water	80 μm

Technical Details for Task 1, Objective 3: The IFT measured from the chemical systems in Task 1, Objective 2 can be used to extract the parameters of the surfactant. The first step is to calculate the maximum surface coverage and the equilibrium adsorption constant based on well-developed isotherm models and equations, [24] such as the Frumkin and Langmuir isotherms, given here respectively:

$$\frac{\Gamma_{eq}}{\Gamma_\infty} = \frac{\kappa c_0}{\kappa c_0 + exp\,(K\Gamma_{eq}/\Gamma_\infty)}. \quad (1)$$

$$\frac{\Gamma_{eq}}{\Gamma_\infty} = \frac{\kappa c_0}{\kappa c_0 + 1}, \quad (2)$$

where Γ_{eq} is the equilibrium surface concentration, Γ_∞ is the maximum surface concentration, and κ is the equilibrium constant, and c_0 is the bulk concentration. The non-zero K in the Frumkin isotherm in Eq. (1) is the constant that considers the molecular interaction. This molecular interaction can be related to van der Waals forces between the hydrocarbon chains of the surfactant molecules and repulsive force from the head groups. When $K = 0$, the Frumkin isotherm reduces to the well-known Langmuir isotherm, which does not consider the interaction between the adsorbed surfactant molecules.

The Gibbs adsorption energy equation is then applied and fitted to the linear portion of the plot for equilibrium IFT versus bulk concentration, when c_0 is close to CMC to obtain Γ_∞, [25, 26]

$$\Gamma_\infty = -\frac{1}{nR_{ig}T}\left(\frac{\partial\gamma}{\partial lnc_0}\right)_{T,C\to CMC}, \quad (3)$$

where R_{ig} is the gas constant, T is the temperature, $n = 1$ for non-ionic surfactant and $n = 2$ for ionic surfactant. Here, γ is the interfacial tension. After Γ_∞ is obtained for each surfactant, Frumkin or Langmuir isotherm is then applied to obtain the equation of state, respectively [24]

$$\gamma = \gamma_0 + n\Gamma_\infty R_{ig}T\left[ln\left(1 - \frac{\Gamma}{\Gamma_\infty}\right) - \frac{K}{2}\left(\frac{\Gamma}{\Gamma_\infty}\right)^2\right] \quad (4)$$

$$\gamma = \gamma_0 + n\Gamma_\infty R_{ig}T\left[ln\left(1 - \frac{\Gamma}{\Gamma_\infty}\right)\right] \quad (5)$$

where γ_0 is the IFT of the surfactant-free interface, Γ is the surfactant concentration at the interface corresponding to γ. Eqs. (4) and (5) are also fitted to the $\gamma_{eq} - C$ plot to obtain κ or K. Alternatively, Eqs. (4) or (5) can be directly used to determine Γ_∞, κ and K simultaneously.

The next step is to use the obtained Γ_∞ and κ to find the diffusivity of surfactant. The transport of surfactant molecules to the macro-scale interfaces, such as the pendant drop, are generally

diffusion-limited [27]. A typical model to predict the surfactant concentration at the interface for diffusion-limited surfactant transport [28] first developed by Ward and Tordai [29] is

$$\Gamma(t) = 2\sqrt{\frac{D_s}{\pi}}\left[c_0\sqrt{t} - \int_0^{\sqrt{t}} c_s\,(t-\tau)d\sqrt{\tau}\right], \quad (6)$$

where c_s is the concentration in the subsurface and D_s is the surfactant diffusivity, t is the time. This model is usually used to extract the diffusivity, D_s for a certain surfactant with concentration below the critical micelle concentration (CMC) for diffusion-limited behavior. To simplify the calculation, the expression of Eq. (6) can be reduced under two approximations. The first approximation is for early times, given by [30]

$$\Gamma(t) = 2c_0\sqrt{\frac{D_s t}{\pi}}, \text{ for } t \to 0. \quad (7)$$

By applying Gibb's adsorption isotherm Eq. (7), the IFT, γ, can be related to Γ through:

$$\gamma_{t\to 0} = \gamma_0 - 2nR_{ig}Tc_0\sqrt{\frac{D_s t}{\pi}}. \quad (8)$$

Eq. (8) describes the decay in IFT at early times of the diffusion process. Eq. (6) can be simplified to another form when IFT approaches equilibrium, and is expressed as

$$\gamma_{t\to\infty} = \gamma_{eq} - \frac{nR_{ig}T\Gamma_{eq}^2}{c_0}\sqrt{\frac{\pi}{4D_s t}}, \quad (9)$$

where γ_{eq} is the equilibrium IFT, and Γ_{eq} is the equilibrium interfacial coverage of the surfactant molecules. The diffusivity of the surfactant molecules, D_s, can be extracted by fitting Eq. (8) and (9) to the dynamic IFT from pendant drop tensiometry, which indicates the rate at which the molecules diffuse into the sublayer of the interface.

When the size of the droplets reduces to the micro-scale, such as those generated in the microfluidic experiments, the transport of surfactant becomes kinetic-limited [31]. This means that the kinetic adsorption time scale is much greater than the diffusion time scale. The rate of adsorption can be extracted by combining the equation of state and rate equation of interfacial coverage, which calculates both the adsorption and desorption rate constants. Using the Langmuir isotherm, the rate equation can be obtained as [32]

$$\frac{\partial}{\partial t}\left(\frac{\Gamma(t)}{\Gamma_\infty}\right) = \beta c_s\left(1 - \frac{\Gamma}{\Gamma_\infty}\right) - \alpha\frac{\Gamma}{\Gamma_\infty}, \quad (10)$$

where β, α are the adsorption and desorption rate constants, respectively Eq. (10) becomes:

$$\frac{\Gamma(t)}{\Gamma_\infty} = \frac{\Gamma_{eq}}{\Gamma_\infty}\left(1 - exp(-t/\tau_{kin})\right). \quad (11)$$

where $\tau_{kin} = \frac{1}{\alpha}\frac{1}{1+\kappa c_0}$, and $\kappa = \beta/\alpha$ based on the Langmuir isotherm. Substituting Eq. (2) into Eq. (11), the equation of state can be modified as a function of time for kinetic-limited transport

$$\gamma(t) = \gamma_0 + n\Gamma_\infty RT\left[ln\left(1 - \frac{c_0}{c_0+(1/\kappa)}\left(1 - exp(-t/\tau_{kin})\right)\right)\right], \quad (12)$$

The rate constants β and α can be obtained by fitting Eq. (12) to dynamic IFT measured from microfluidic experiments with extracted values of Γ_∞ and κ.

Technical Details for Task 1, Objective 4:

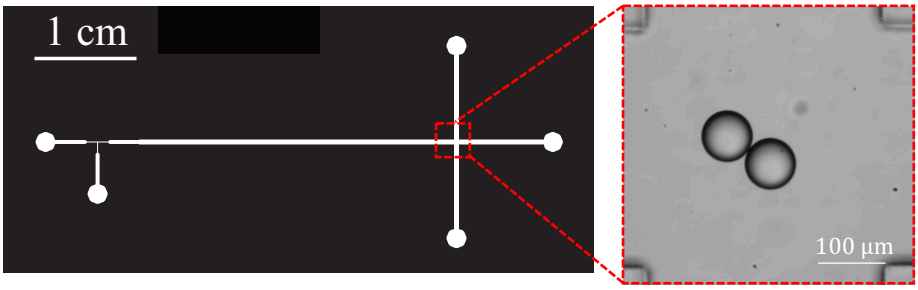

Figure 3. (Left) Microfluidics Stokes' trap device (Right)Two trapped droplets interacting at the stagnation point of the cross-slot of a microfluidics Stokes-trap device.

The droplet coalescence experiments are performed using a microfluidic Stokes-trap device (**Figure 3**). Droplets are generated upstream and later trapped downstream in the cross-slot region of the device. By adjusting the pressure to each channel, a droplet is held inside the trapping region, while new droplets are allowed to collide and coalescence with the trapped droplet. Whether the two droplets coalesce or not are recorded. Film drainage time between the two droplets is extracted from the recorded video for model bilgewater systems. Given the results of dynamic IFT and surfactant concentration from the previous part of the project, the results here provide the fundamental understanding of the relation between the IFT and the film drainage time between the two coalescing droplets.

Based on the original design of the 4- and 6-channel, a serpentine-shaped channel has now been added right after the injection point, including all continuous and one dispersive channel as shown in **Figure 4**. The purpose of this serpentine shape is to increase the length of the channel and provide extra resistance to the flow, such that the flow rate can be reduced. The serpentine channel was designed with two different lengths for testing. The experiment performed using the shorter length of serpentine channel has shown clear decrease of the droplet velocity and several droplets have been successfully trapped, which verifies that the modified design works better for the oil-in-water trapping. The systems studied for the droplet coalescence experiments are listed in **Table 3**.

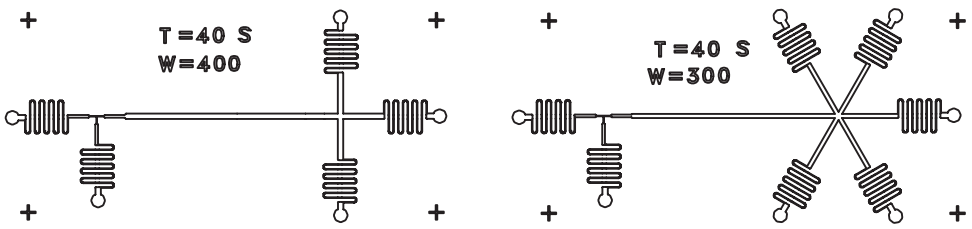

Figure 4. Modified designs of the (left) 4- and (right) 6- channel Stokes trap microfluidic devices. T=40 indicates that the width of the T-junction channel is 40 μm, W=400 indicates the width of the cross-slot channel is 400 μm. The serpentine shapes have been added next to each inlet of the channel, such that the total length of the four continuous and one dispersive phase channels are all increased. The S in the design indicates that this is a shorter version of the serpentine channel. In addition to the designs shown here, an additional geometry with increased length of the serpentine portion was also prepared.

Table 3. Chemical Compositions Studied for Task 1, Deliverable 4

Water Phase	Oil Phase	Surfactant + Phase	Concentration	Oil-in-water or water-in-oil
Distilled Water	NSBM#4	Detergent Mix in water	0 ppm, 10 ppm, 50 ppm	o/w
			0 ppm	w/o
Distilled Water	LMO	Span 80 in LMO	500 ppm, 1000 ppm	o/w
Distilled Water	LMO	Type 1 in water	50 ppm 100 ppm	o/w
			0 ppm	w/o
Distilled Water	LMO	SDS in water	1000 ppm	w/o and o/w

Technical Approach for Task 2, Objective 1: The droplet stability is determined for each system via the measurement of emulsion turbidity in centrifuge tube, as shown in **Figure 5**. Samples are emulsified using a Carderock advised protocol. The emulsifying equipment is an IKA Ultra Turrax T-25 Homogenizer. Samples are blended in a 50 mL centrifuge tube blending chamber for 2 minutes at 25,000 rpm. For the Stability Tests (e.g., **Figure 6**), transparent vials containing the sample are observed over a period of days using a camera and image analysis. The change in the opaqueness (turbidity) of the sample is used to determine the destabilization time for a variety of simulated bilgewater and model systems.

Mesoscopically, stability is also determined using size distribution measurements. Stable emulsions will contain many small droplets, while destabilized emulsions will contain larger, more coalesced droplets. Two methods for determining the droplet size distribution are used in this work: Laser Diffraction Particle Analyzer (Microtrac Bluewave) and direct visualization using brightfield microscopy. Code was written to track the edge of the droplet in each image, to determine size. Results from the size distribution analysis for both methods is discussed later in the Results section.

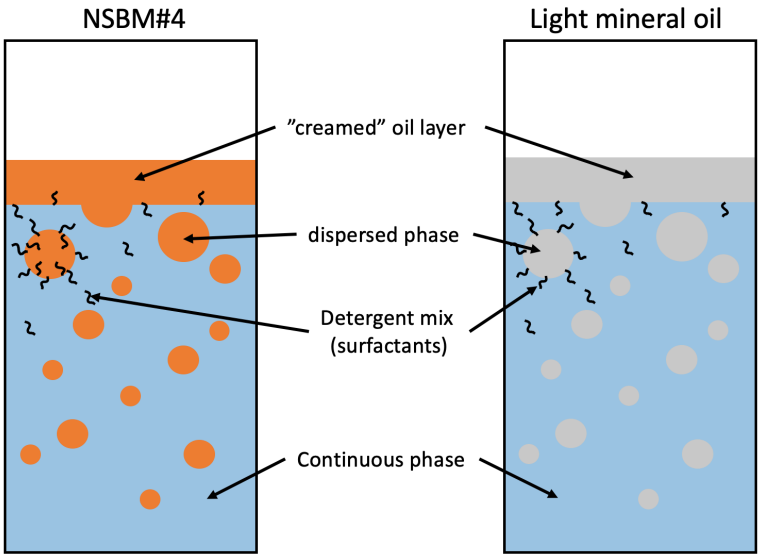

Figure 5. Schematics of the static stability test. Two different systems are tested: NSBM#4 in water (left) and LMO in water (right). Detergent mix is added to the water phase for both systems.

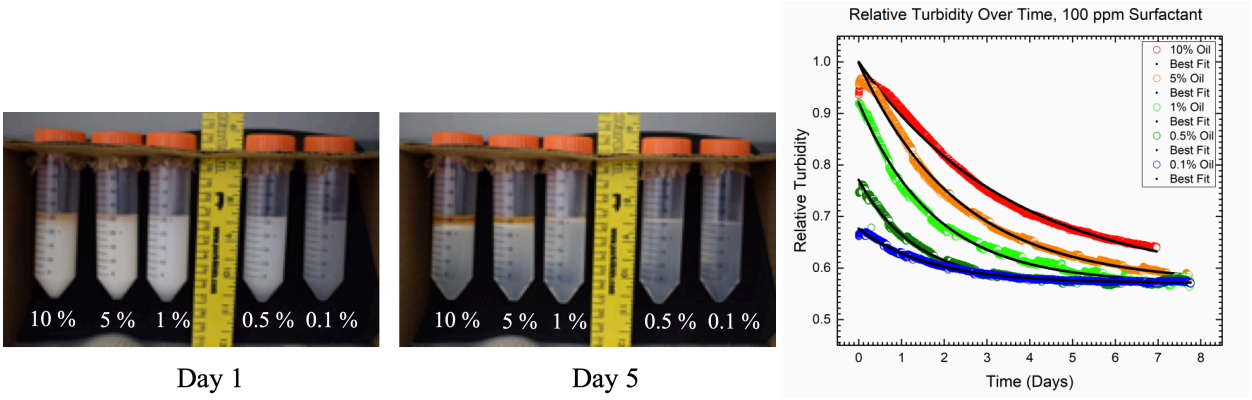

Figure 6. (Left) Stability test shows phase separation due to destabilization of the emulsion. The oil:water ratio of the samples (from left to right) are 10%, 5%, 1%, 0.5%, and 0.1%. Each contain 10 ppm of the SERDP detergent mix. (Right) Relative turbidity of five similar samples, with 100 ppm SERDP detergent mix, over time. Fits are to an exponential decay, resulting in a timescale for destabilization. Please note that these curves are normalized by the highest turbidity observed (10% oil at time 0), to illustrate the difference in emulsion decay times across multiple o:w ratios.

Technical Approach for Objective 2: Viscosity of the emulsion as a function of shear rate is determined using a rotational rheometer (AR-G2 TA Instruments) as shown in **Figure 7** for the simulated bilgewater and model systems. Viscosity as a function of shear rate is needed to calculate the dimensionless cylinder speed (Reynolds number) in later objectives 3 and 4, based on the global shear rate, as well as serves as a metric for emulsion stability under shear. Systems with hysteretic, or history-dependent, viscosity profiles indicate macroscale phase separation. Results of emulsion destabilization are supported with droplet size distribution measurements.

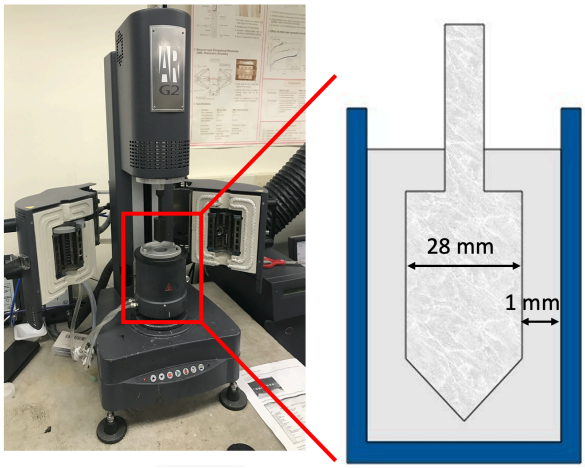

Figure 7. (Left) Rheometer for determining dependence of viscosity on shear rate or shear stress for non-Newtonian fluids. (Right) Schematic of the rheometer with a stator and rotator.

Technical Details for Objective 3: The pre-prepared emulsion samples were prepared in two major varieties, a simulated bilgewater variety designed to closely replicate bilgewater using many of the same ingredients found onboard marine vessels, and a "model" variety employing less chemically complex substitutes for shipboard ingredients. The simulated emulsion system aligned with specifications provided by the SERDP program and Naval Surface Warfare Center Carderock Division. The Navy Standard Bilge Mix (NSBM#4) and detergent mix (**Table 1**) were specified as the surfactant mixture pre-loaded into the continuous water phase. For the model system, the NSBM#4 in the dispersed phase is replaced by pure Light Mineral Oil. A detailed list is shown in **Table 4**. Note that distilled water is used for all the experiments.

All emulsion samples used in following pre-prepared Taylor Couette experiments were blended with a rotor-stator homogenizer (IKA: T-25 digital Ultra-Turrax) for a fixed duration (120 seconds) and at a fixed homogenization rate (20,000 rpm). For Taylor-Couette (TC) cell experiments, the size of the TC cell dictated a need for 2L of emulsion sample to be prepared. In this case, two batches of 1L each are prepared back to back in a pair of 1L glass jars due to the volume constraints of the T-25, then mixed thoroughly in a single 2L beaker. The 2L volume of sample required for the TC cell also limited the choice of standard emulsion recipe due to limited oil supplies, so only the SERDP-recommended concentration of oil (0.1% vol/vol) and surfactant (100 ppm vol/vol) were utilized.

Table 4. Experiments Performed and Chemical Composition of Emulsions Studied in Task 2. Note that several of these experiments have now been performed with multiple replicates.

Experiment	Oil	Water	O:W (% v/v)	Surfactant	Surfactant Concentration (ppm v/v)
Static Stability Test Objective 1	NSBM#4	Water	0.1, 0.5, 1, 5, 10, 11	SERDP	0, 1, 10, 50, 100
	NSBM#4	Water	0.1, 0.5, 1, 5, 10	LAS	100
	NSBM#4	SSW	0.1, 0.5, 1, 5, 10	SERDP	100
	NSBM#4	SSW	0.1, 0.5, 1, 5, 10	AES	100
	LMO	Water	0.1, 0.5, 1, 5, 10	SERDP	0, 1, 10, 50, 100
	LMO	Water	0.1, 10	LAS	100
	LMO	Water	0.1, 0.5, 1, 5, 10, 20	AES	1, 10
	LMO	SSW	0.1, 0.5, 1, 5, 10	SERDP	100
Rheometry: Objective 2	NSBM#4	Water	0.1, 0.5, 1, 5, 6, 7, 8, 9, 9.5, 10, 11	SERDP	0, 1, 10, 50, 100
	NSBM#4	Water	0.1, 0.5, 1, 5, 10	LAS	100
	NSBM#4	SSW	0.1	SERDP	100
	LMO	Water	0.1, 10	SERDP	100
	LMO	Water	0.1, 10	LAS	100
	LMO	Water	0.1, 10, 20	AES	10
	LMO	SSW	0.1, 10	SERDP	100
TC Cell: Objectives 3 and 4	NSBM#4	Water	0.1	SERDP	100
	NSBM#4	Water	0.1	LAS	100
	NSBM#4	SSW	0.1	SERDP	100
	NSBM#4	Water	0.1	AES	100
	LMO	Water	0.1	SERDP	100
	LMO	SSW	0.1	SERDP	100

Taylor-Couette Experiments. The Taylor-Couette (TC) cell used in these experiments is a custom-designed vertical concentric cylinder, with an inner cylinder constructed of anodized aluminum of diameter, $D_{in} = 13.54 \pm 0.01$ cm and an outer cylinder made of borosilicate glass of diameter, $D_{out} = 15.20 \pm 0.01$ cm. The annulus radial width between the cylinders d is 0.84 cm and the annulus gap height h is 51 cm. More information on the construction and operation of this device can be found in previously published work [3, 5]. In practice, 2L of prepared simulated bilgewater emulsion mixture is sufficient to submerge the inner cylinder and allow for normal operation of this device without the optional radial injection system. This mixture, once blended, is added into the mixing chamber of the cell via plastic tubing that feeds liquids into the bottom of the annulus. A detailed exterior image of the TC cell, including the transfer apparatus, is included in **Figure 8**.

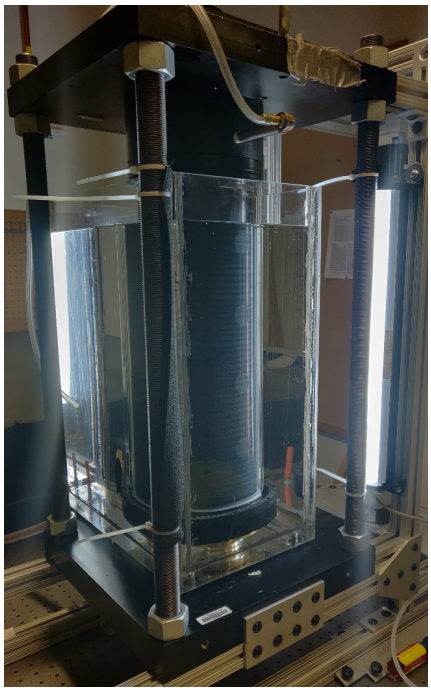

Figure 8. Custom designed Taylor Couette Cell

The types of experiments conducted for this work are divided into two primary categories: stepwise experiments and ramp experiments. These categories are defined by the control of cylinder rotation rate over the course of the experiment. For stepwise experiments, the simulated bilgewater emulsion mixture is exposed to a series of mixing speeds within the annulus of increasing strength, with each specific mixing speed being maintained for a fixed duration. Stepwise experiments featured fixed intervals of 10 minutes for each mixing step. The Reynolds number of the rotational flow generated within the annulus from rotation of the inner cylinder was used as the metric for quantifying mixing strength. Experiments consisted of three distinct steps of increasing mixing strengths, subjecting the emulsion to different flow mixing conditions in the TC cell, first step of Re_{in} = 650 (laminar wavy vortex flow), second step of Re_{in} = 2000 (turbulent wavy vortex flow) and third step of Re = 4000 (turbulent Taylor vortex flow). Several combinations of these steps were employed across multiple iterations of stepwise experiments to determine the impact of exposure to mixing environments of differing strength on the stability of bilgewater emulsions and the evolution of emulsion droplet size distributions. Ramp experiments consisted of a quasistatic steady increase of inner cylinder rotational speed, allowing for a steady progression and development of a variety of flow sates of varying mixing strength, subjecting the solution to steadily increasing shear. Ramp experiments were conducted across a range of Re_{in} from ~300 to ~4000, encompassing an array of flow states including all three previously chosen for stepwise experiments.

For both stepwise and ramp experiments, 20 mL samples of the emulsion mixture were extracted from the annulus at predetermined times during the course of the experiment. Two samples were taken at the beginning of each experiment. Droplet size distributions were generated immediately from one of these according to the procedures outlined in the next sections, while the other was left to sit undisturbed for the duration of the experiment. Further samples were extracted at the

conclusion of each discrete mixing step in the case of stepwise experiments, and at the conclusion of the experiment in the case of ramp experiments. In both cases, droplet size distributions were generated from all samples collected during the experiment, as well as the sample collected at the beginning and left undisturbed, according to the procedures outlined above. This was done to ensure that the effect of time alone on the evolution of bilgewater emulsion droplet size distribution could be isolated from the effects of exposure to Taylor-Couette mixing environments.

Droplet size distribution. The samples collected from the experiments described in the previous sections were used to determine the droplet size distribution of the emulsion, which is the primary method used to determine the influence of rotational shear or Taylor-Couette mixing on bilgewater emulsion stability. Different emulsion samples were taken both before and after experimentation from the same pre-mixed batch. Two different methods for measuring droplet size distributions were used for this purpose. The first and most reliable being laser diffraction particle size analysis, conducted with a Bluewave Laser Diffraction Particle Size Analyzer (Mictrotrac®). Samples taken from the same experiment were tested at the same time, and both number distribution and volume distributions were collected in all cases.

The second method used was optical microscopy, employing an Olympus IX-73 Inverted Microscope with 60X objective and mounted camera to capture close-up images of emulsion droplets. These images were taken for all stages of sample extraction for all experiments. In order to keep the emulsion droplets under study within the lens's depth of field, and thus visible, a series of custom-designed circular wells of 50 micrometer depth, made of Polydimethylsiloxane (PDMS) and affixed to glass microscope slides, were used. Between ten and twenty images, depending on the diluteness of the sample, were taken at a variety of depths in order to produce a statistical confidence interval for droplet size analysis for each emulsion sample. Matlab-based image analysis was used to detect droplets over a range of diameters and to produce a histogram of total droplets found in the series, distributed incrementally by a scale of one image pixel. **Figure 9 (A) & (B)** shows an example of a microscopy image taken of an emulsion sample undergoing the droplet-counting procedure and includes a representative histogram (see **Figure 9 (C)**) produced from that procedure. These histograms are comparable to the number distributions produced by the laser diffraction system, although volume distributions have been found to be more useful for this work.

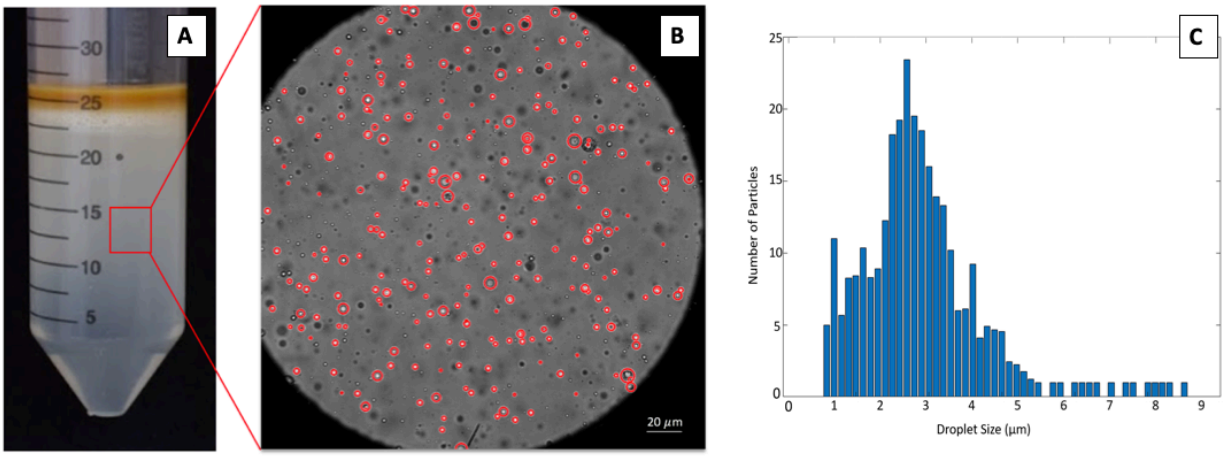

Figure 9. An example of a vial (A) and microscopy image undergoing droplet counting (B), with custom Matlab code modified to display the droplets found during one cycle in red, and an example histogram generated for this image (C).

Technical Details for Objective 4:

Oil injection calibration. The custom designed TC cell used in the following experiments consists of an inner cylinder with 16 injection ports evenly distributed axially and azimuthally. The non-protruding injection ports were covered by contour matched 3d printed covers such that the flow profile is not affected during the experiments (the design can be found in [3, 5]). To make surfactant solutions, 100 ppm (vol/vol) SERDP surfactant was added to 2L beaker filled with 1L of water and mixed by shaking them vigorously for 10 minutes. The process was repeated to make 2L of water-surfactant solution. The solution is then transferred to the annulus of TC cell by the way of tubing attached to the base of the cylinder assembly as seen in **Figure 8**. Since we needed to inject 0.1% oil (vol/vol), the quantification of injected mass into annulus was performed by a calibration curve with pressure as a function of injection duration. The flow rate of the individual injection ports and time required for injection was determined using the calibration experiments.

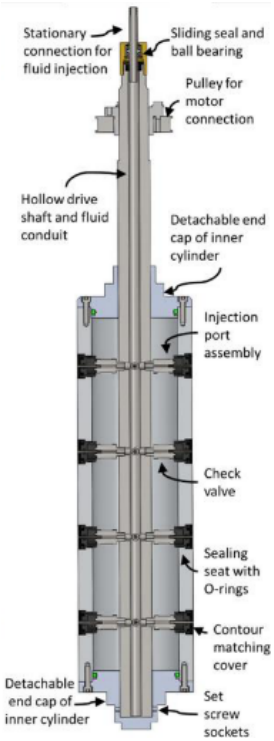

Figure 10. Schematic of the TC inner cylinder showing the injection system

Flow rates were measured for pure light mineral oil at a pressure of 15 psi at different injection times (2, 5, 7.5 10, 15 seconds). For easier sample collection, the outer covering and the port covers of the inner cylinder were removed to measure the amount of fluid exiting each port of the cylinder (**Figure 10**). Flow homogeneity between ports was determined by measuring mass injected from each port and measured using electronic weighing scale. The injection measurements were

repeated 3 times for each time interval to create a 95% confidence interval. The lower pressure of 15 psi was chosen due to low injection amount (0.1% vol/vol) of the light mineral oil required. The total mass injected was plotted as a function of time with statistical confidence interval in **Figure 11**.

Flow rate and total injected mass can be controlled independently by varying the driving pressure of the injection time. After the injection mass data was collected, it was fitted to obtain an equation relating the injection time and the total mass injected. This equation is further used to determine the amount of time required to inject (0.1% vol/vol) of light mineral oil directly into a pre-established flow condition containing water-surfactant mixture at 15 psi pressure.

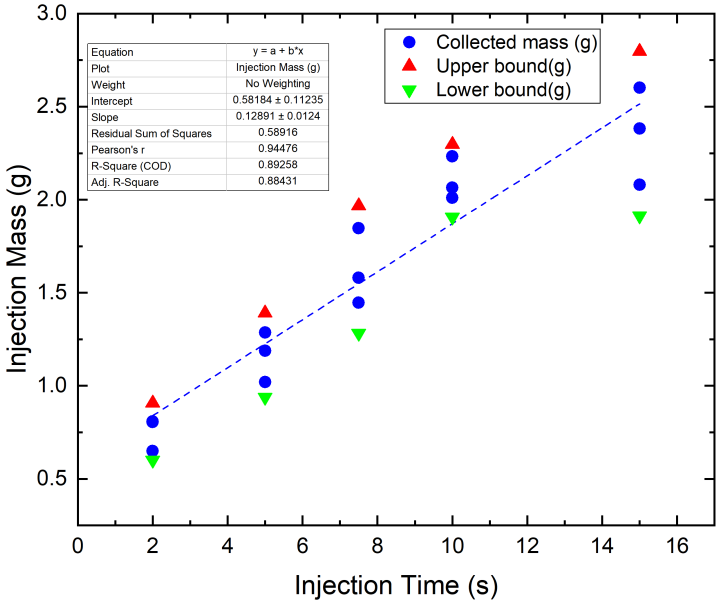

Figure 11. Total mass injected as a function of time for light mineral oil at 15 psi injection pressure.

In-situ TC experiments. The in-situ experiments were conducted in a similar stepwise manner as described earlier. First the water-surfactant solution was loaded into the annulus of the Taylor Couette cylinder as described earlier. Second, a higher order flow state was established by rotating the inner cylinder at a $Re_{in} = 6000$ as higher mixing speeds are required. The oil was then injected into the annulus of the cell at this Re_{in}. After injection, the flow state was maintained for a fixed duration of time (20 minutes in this case) to allow the oil droplets injected to mix into the solution. Later the regular stepwise experiments were conducted, but instead of stepping up in mixing speed, the inner cylinder speed was stepped down to $Re_{in} = 4000$ (turbulent Taylor vortex flow), $Re_{in} = 2000$ (Taylor wavy vortex flow) and finally to $Re_{in} = 650$ (laminar wavy vortex flow) and maintain for 10 minutes at each step. Samples of 20 ml were collected after each flow step using the tube connected to the base of the cylinder. The samples were analyzed by performing microscopy analysis and laser size diffraction analysis as described in the previous sections.

There are five sets of experiments conducted in this objective. The first experiment consisted of jar tests with 0.1% NSBM #4 and 100 ppm SERDP surfactant performed to check the ability of the solution to form emulsion at low shear rates offered by the TC cell. The jar tests were conducted

in a VELP Scientifica JTL4 Flocculator at 300 RPM for 30 min and later samples were tested in laser diffraction size distribution and optical microscopy. The second experiment was performed in a TC cell with the same solution composition of 0.1% NSBM #4 & 100 ppm SERDP surfactant in distilled water solution. This solution was directly loaded into the annulus of the cell. The inner cylinder was first rotated at a high mixing speed (turbulent Taylor flow) and maintained at this speed for 20 minutes. The mixing speed was later stepped down to turbulent wavy flow and laminar wavy flow, where the flow was maintained for 10 minutes and samples were collected at the end of each step speed. In the third experiment, comparison studies were conducted between different oil concentration, different type and concentration of surfactants to determine an optimum composition for the stable emulsion formation in the TC cell. It consisted of four solutions (higher oil (1% NSBM#4), lower surfactant (10 ppm SERDP), higher oil & lower surfactant (1% NSBM#4 & 10 ppm SERDP) and lastly higher oil with type 1 surfactant (1% NSBM#4 & 10 ppm type 1). For the fourth experiment, a solution with much higher oil concentration of 2% NSBM #4 with 100 ppm SERDP in distilled water was loaded in the annulus of the cell and similar step wise mixing experiments (as described above for second experiment) were performed. The collected samples were also similarly analyzed using laser diffraction particle sizing and optical microscopy. The fifth experiment was performed as a proof of concept to observe the formation of stable emulsions using a concentrated (higher – 1% NSBM) solution blended in a rotor-stator homogenizer (IKA: T-25 digital Ultra-Turrax) for a fixed duration (120 seconds) and at a fixed homogenization rate (20,000 rpm). 200 ml out of the prepared 500 ml solution was mixed in a 100 ppm SERDP surfactant water solution to make a final 0.1% NSBM, 100 ppm SERDP 2L solution.

Results and Discussion

Task 1, Objective 1: Surface Treatment of Microfluidic Devices

Three different methods were proposed and tested for the device surface treatment. Method 1: The PDMS was coated with PVA (Polyvinyl alcohol) solution (adapted from Trantidou et al. [33]). The PVA coated device was tested by injecting Synthetic Sea Water (SSW) as continuous phase and sheath flow, diesel as dispersed phase. The result showed that we were able to successfully generate the diesel droplets in the SSW; instead, the channel appeared to be not completely coated with PVA and diesel droplets adhered to the channel walls. Method 2: The hydrophilicity of PDMS was varied by mixing HEMA (hidroxietilmetacrylate) with PDMS before fabrication of the devices (adapted from Rigat-Brugarolas et al. [34]). After curing of the PDMS, the wettability of both SSW and marine oil was tested by comparing the contact angle of 20 µl droplets for both liquids. The result showed that the contact angle of the water droplet is still larger than that of the diesel droplet, and hydrophilicity is not enhanced. Method 3: A fully bonded device was exposed to a second oxygen plasma treatment with 20 W for over 5 minutes (adapted from Tan et al. [22]). After the treatment, the device was immediately tested by injecting SSW as continuous phase and sheath flow, diesel as dispersed phase. The result showed that we were able to successfully generate the diesel droplets in the SSW for the first 15 - 20 minutes (see **Figure 12**), but the device surface recovered to hydrophobic instantly after this initial time period. Methods 1 and 3 have shown to successfully generate diesel droplets in SSW phase, but the hydrophilicity of the device is still currently unstable. Particularly, for method 3, a higher power plasma treatment (i.e. 100W) is used to keep the treated PDMS hydrophilic up to six hours. Therefore, method 3 has been the main focus of the treatment method.

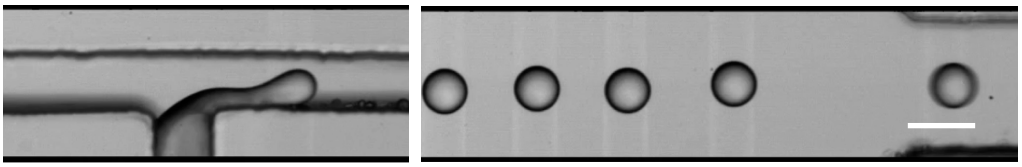

Figure 12. Successful generation (left) and flow (right) of droplets of SERDP diesel oil in a continuous phase of synthetic sea water, using "Method 3" as described. In brief, a fully bonded device was exposed to a second oxygen plasma treatment with 20 W for over 5 minutes, in order to change the wettability of the channel walls and enable oil-in-water drops. Scale bar is 100 micrometers.

To further modify the method 3, the microfluidic chip is bonded with PDMS coated glass slide instead of being bonded directly to the glass, which makes it possible for all the channel walls to receive hydrophilic treatment. The bonded chip is then exposed to a second oxygen plasma treatment with 100 W for 10 minutes [22] subject to oxygen flow. After the treatment, the device is immediately stored in DI water under vacuum to remove all the air in the micro channels. The device is then tested after 5 days and the result show that diesel oil mix droplets are successfully generated in continuous SSW phase and the device remains hydrophilic for at least 2 hours, which allows us to take videos of droplets from various tensiometers.

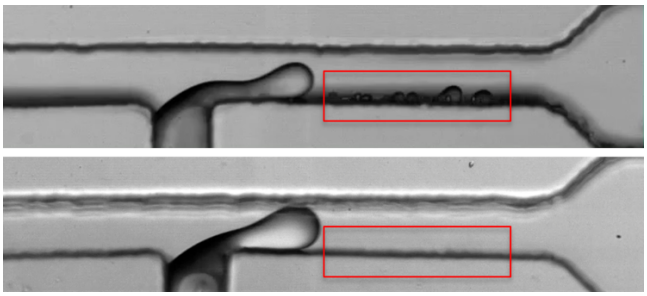

Figure 13. (Top) Device is treated in 20 W plasma for 15 min right before the test; (Bottom) Device is treated in 100 W plasma, with oxygen flow at 300 sccm, for 10 min, and is stored in DI water under vacuum for at least 5 days before the test.

This method has been further modified and optimized for best surface treatment for our device: The bonded PDMS device is now exposed to a second oxygen plasma treatment with *150 W* for *15 minutes* subject to oxygen flow at *300 sccm*. After the treatment, the device is immediately stored in DI water under vacuum at least for 7 days. The treated device is then tested and the result shows that diesel oil mix droplets are successfully generated in continuous SSW phase and the device remains hydrophilic for over 4 hours, which provides the sufficient time for running one dynamic IFT experiment. In addition, the wettability of the device has been significantly improved with no droplets attached on the channel wall as shown in **Figure 13**. The microfluidic channel length has also been increased 3 times, so that the flow velocity is now reduced approximately 3 times compared to previous channel design with the same input pressure. The experiments are now recorded at a more reasonable 40,000 fps and the edge of the droplets are clear and detectable by Matlab.

Task 1, Objective 2: Dynamic IFT of Microscale Droplet using Microfluidics

Measurements of dynamic IFT of detergent mix added in SSW as aqueous phase with NSBM #4 as the oil phase have been performed [35] as shown in **Figure 14**. For all the cases, the time of decay in IFT of "no surfactant" condition suggests that the oil mix contains some surfactants, likely due to different chemical components in diesel fuels. When the surfactant is added at 25 ppm (below CMC) and 100 ppm (above CMC), there is clear decrease in equilibrium IFT, which shows the effect on the IFT from the addition of surfactant. In most cases, the equilibrium IFT from microfluidics agrees with the measurement from pendant drop over long-time scale in the inset. However, the IFT drops significantly within 2 seconds for microfluidic droplets, while the IFT decays at order of 100 seconds from pendant drop measurements. Given the fact that the diameter of droplets is about 75 μm in microfluidics and 2 mm for pendant drop, the rate of decay of dynamic IFT is apparently dependent on the size. This size-dependence has also been observed recently by our group for water-in-fuel systems [36] and is likely due to the difference in timescales of surfactant transport. This difference in IFT timescales could have important implications for bilgewater treatment. Smaller, micrometer-sized droplets are more relevant to bilgewater treatment than millimeter-sized droplets, and the measurements from the microfluidics device are likely a more accurate measure of the true interfacial tensions of bilgewater emulsions. More interestingly, the IFT decays even faster (within 1 second) for oil-in-water compared to water-in-oil (within 2 seconds) for micro-scale droplets as shown in **Figure 14** (left), which indicates a phase dependency of the surfactant transport. On the contrary, the rate of decay does not change significantly for pendant drop IFT when the surfactant is added to outer phase in **Figure 14** (right). Here, lower equilibrium IFT of 25 ppm and 100 ppm detergent mix of oil-in-water are observed in microfluidics compared to the values of pendant drop at the same concentration. In general, the equilibrium IFT is mostly dependent on the bulk concentration, and this indicates that the IFT for oil-in-water pendant drop measurements has not reached equilibrium values yet even at 500 seconds.

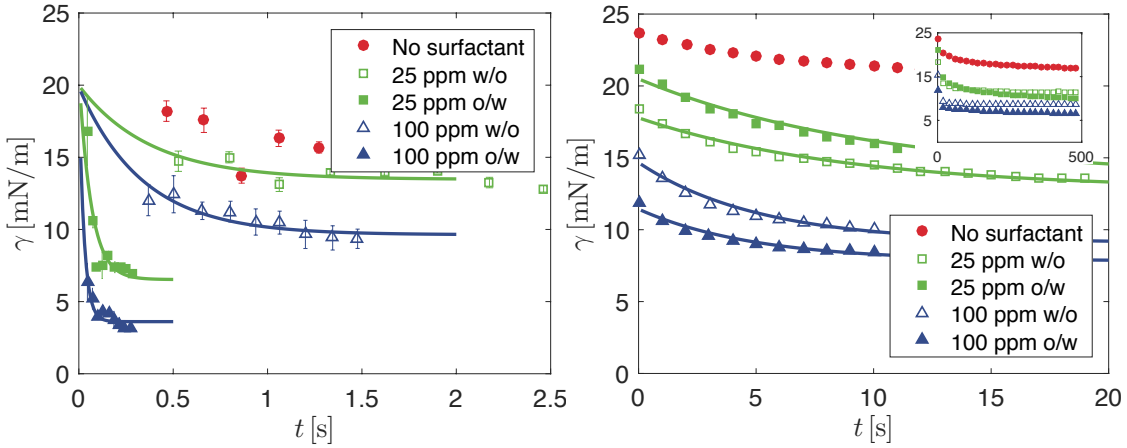

Figure 14. Dynamic IFT *(γ)* of droplets as a function of time (t) with no surfactant, 25 ppm and 100 ppm detergent mix for water-in-oil and oil-in-water using (left) microfluidic tensiometry and (right) pendant drop measurements. The inset figure shows the IFT of a pendant drop over long-time scale. The time scale for the decay in IFT of each experiment is extracted by fitting the $\gamma - t$ curve with the exponential function, $\gamma = a\,exp(-t/\tau) + b$, shown as the lines in the plot.

In addition to the experiments using simulated detergent mix, we have also conducted experiments using model surfactant to answer fundamental questions about the observed dynamic IFT behavior. The results in **Figure 15** show the dynamic IFT of anionic surfactant AES in SSW and NSBM#4 as the oil phase.

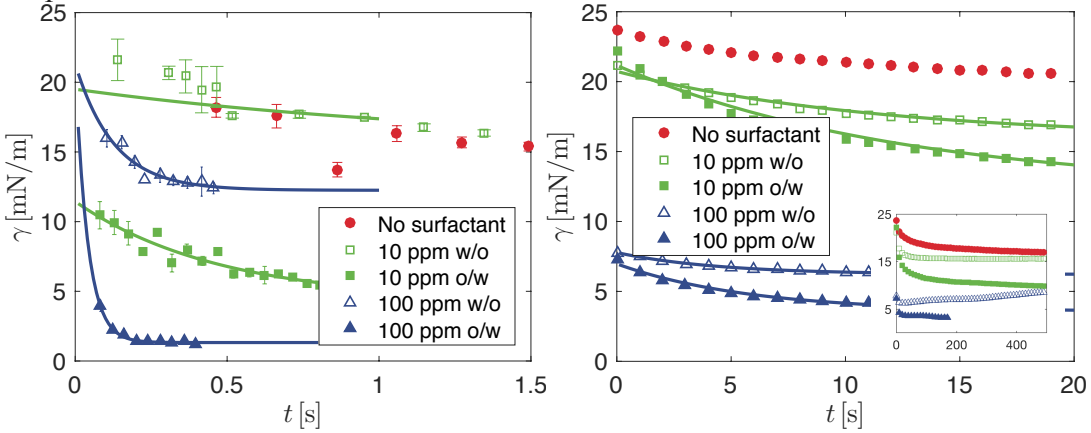

Figure 15. Dynamic IFT (γ) of droplets as a function of time (t) with no surfactant, 10 ppm and 100 ppm AES for water-in-oil and oil-in-water using (left) microfluidic tensiometry and (right) pendant drop measurements. The inset figure shows the IFT of a pendant drop over long-time scale. The time scale for the decay in IFT of each experiment is extracted by fitting the $\gamma - t$ curve with the exponential function, $\gamma = a\,exp(-t/\tau) + b$, shown as the lines in the plot.

Similar to the results of detergent mix, the IFT also decays faster for micro-scale droplets compared to the pendant drop. Also, the faster rate of decay (within 1 second) is observed for 10 ppm o/w and 100 ppm o/w in microfluidics when the surfactant is in the outer phase, which provides the evidence that the size and phase dependency of the decay in IFT is not unique for detergent mix but is generally observed for different surfactants.

Table 5. Time scale of dynamic IFT extracted from pendant drop and microfluidic

	Pendant Drop				Microfluidics			
Surfactant	**Detergent Mix**		**AES**		**Detergent Mix**		**AES**	
C (mol/m^3)	0.0887 (25 ppm)	0.354 (100 ppm)	0.025 (10 ppm)	0.25 (100 ppm)	0.0887 (25 ppm)	0.354 (100 ppm)	0.025 (10 ppm)	0.25 (100 ppm)
τ_{in_exp} (s)	14.17	5.29	11.97	4.45	0.378	0.24	0.17	0.09
τ_{out_exp} (s)	16.15	6.85	14.41	5.82	0.065	0.027	0.06	0.03

The time scales of the decay in IFT extracted from both pendant drop and microfluidics measurements are listed in **Table 5**, where τ_{in_exp} and τ_{out_exp} are the time scale for surfactant in the inner and outer phase from the experiments, respectively. The values of τ_{in_exp} and τ_{out_exp} shown in **Table 5** are quantitatively consistent with the observation from the dynamic IFT measurement in **Figure 14** and **Figure 15,** in which the rate of decay of IFT for pendant drop does not change significantly when the surfactant is in the outer phase compared to the surfactant in the inner phase for both surfactants. However, for microfluidics experiments, τ_{out_exp} is clearly smaller than τ_{in_exp}, which indicates the significant change of the time scale of decay for surfactant in the outer phase versus in the inner phase.

Task 1, Objective 3: Characterization of Surfactant

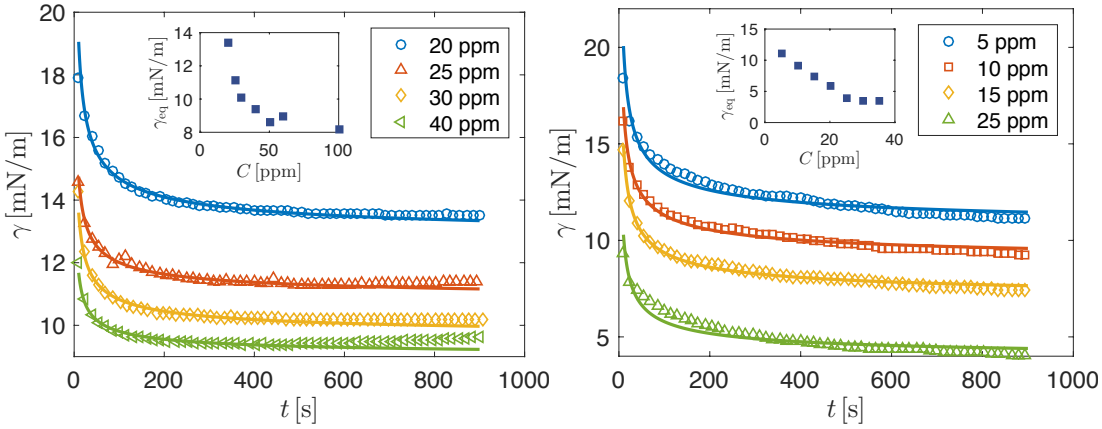

Figure 16. Pendant drop measurement of dynamic IFT of NSBM#4 oil mix in SSW with (left) detergent mix and (right) AES at various concentration. The diffusivity, $D_{C<CMC}$, of each experiment is extracted by fitting the $\gamma - t$ curve with the function, $\gamma = \gamma_{eq} + \lambda t^{-1/2}$, shown as the lines in the plot. The inset figures show the equilibrium IFT for each corresponding curve as a function of bulk concentration, C, which gives the CMC of each surfactant.

In order to study the mechanism of the surfactant transport, the surfactant parameters, such as the critical micelle concentration (CMC), maximum surfactant surface coverage, Γ_∞, adsorption constant, κ, and the diffusivity of the surfactant molecules below CMC, $D_{\mathrm{C<CMC}}$ are extracted based on the IFT measurements [37]. The parameters can be obtained using the Gibbs energy equation, Langmuir or Frumkin isotherm and fit the equation of state to the IFT measurements from the inset of **Figure 16.** Based on the isotherm models discussed in Technical Approach section, we are able to obtain the maximum surface concentration and the ratio between the desorption and adsorption for detergent mix at the interface between SSW and SERDP oil. These two values are calculated based on the pendant drop experiments and they are the key parameters to extract the diffusivity and adsorption/desorption rate from the pendant drop measurement and microfluidics IFT experiments, respectively. We can calculate the adsorption rate and desorption rate based on the time scale of decay fitted from the dynamic IFT curve of the microfluidics. In particular, we use Langmuir's kinetic equation assuming kinetic-limited adsorption/desorption for micro droplets. The obtained values of adsorption/desorption rate from water-in-oil and oil-in-water experiments are compared with each other.

Table 6. Surfactant parameters obtained from pendant drop tensiometry

Surfactant	Detergent Mix	AES
M_w (g/mol)	300	420
Γ_∞ (mol/m^2)	1.52×10^{-6}	2.53×10^{-6}
κ (m^3/mol)	380	904
CMC (mol/m^3)	1.77×10^{-1} (50 ppm)	6.25×10^{-2} (25 ppm)
$D_{\mathrm{C<CMC}}$ (m^2/s)	3.19×10^{-11}	1.9×10^{-10}

The calculated parameters of detergent mix and AES are listed in **Table 6**, where M_w is the molecular weight for each surfactant. In particular, since the detergent mix is a mixture surfactant with multiple types of surfactant molecules as listed in **Table 1,** the molecular weight of it is estimated as the value of a typical surfactant. The extracted values of Γ_∞ for both surfactants are in the reasonable order of magnitude for surfactant molecules, while $D_{C<CMC}$ of detergent mix is in one order of magnitude smaller than the typical value ($10^{-10}\ m^2/s$). The deviation of this is probably due to the unprecise M_w used in the calculation, which is difficult to obtain for mixture of surfactants. If the surfactant transport is diffusion-controlled (i.e. milli-scale droplets), the value of $D_{C<CMC}$, can be used to calculate the diffusion time scale $\tau_D = \left(h_s^3 h_p\right)^{1/2}/D_{C<CMC}$, where h_s and h_p are the spherical and planar diffusion length scale, respectively. It is clear that the due to higher value of κ for AES than detergent mix, the surfactant molecules of AES are more active than that of detergent mix.

With the calculated Γ_∞ and κ for both surfactants, the adsorption and desorption rate constants can also be obtained using the Langmuir equation and dynamic IFT measured as shown in **Figure 14** & **15**. The extracted adsorption, k_{ads}, and desorption, k_{des}, rate constant for both detergent mix and AES in inner and outer phase of microfluidics are listed in **Table 7.** Clearly, all cases show that the rate constants for surfactant in the outer phase are much larger than that in the inner phase.

The adsorption, k_{ads}, and desorption, k_{des}, rate constants indicate the ability of surfactant transport into the interface is kinetic-limit, and, therefore, are of importance in predicting the IFT time scale of the decay of the bilgewater system. If the surfactant transport is kinetic-controlled (i.e. micro-scale droplets), k_{ads} and k_{des} can be used to predict the adsorbing time scale $\tau_{\mathrm{k}} = 1/(k_{\mathrm{des}} + k_{\mathrm{ads}}C)$. The values of $\mathrm{k_{ads}}$ for all the cases extracted are within the reasonable range of order of magnitude $10^0 \sim 10^2\ \mathrm{m^3/mol \cdot s}$ for typical surfactants.

Table 7. Surfactant adsorption and desorption rate from microfluidic experiments

Surfactant		**Detergent Mix**		**AES**	
C $\mathbf{(mol/m^3)}$		0.0887 (25 ppm)	0.354 (100 ppm)	0.025 (10 ppm)	0.25 (100 ppm)
$\boldsymbol{k_{\mathrm{ads}}}$ $\mathbf{(m^3/mol \cdot s)}$	Inner	54.5	5.61	95.2	88.2
$\boldsymbol{k_{\mathrm{des}}(1/s)}$	Inner	0.143	0.0147	0.105	0.0975
$\boldsymbol{k_{\mathrm{ads}}}$ $\mathbf{(m^3/mol \cdot s)}$	Outer	299	96.2	221	171
$\boldsymbol{k_{\mathrm{des}}(1/s)}$	Outer	0.786	0.253	0.244	0.189

The extracted values of the adsorption rate constant are smaller when the surfactant is inside the droplet, suggesting a larger energy barrier for the surfactant molecules. Though several possible factors can influence the energy barrier for adsorption, the most likely one is that the molecules need to be in the correct orientation for adsorption. The surfactant molecules will prefer to diffuse back to the bulk to rearrange themselves rather than reach the adsorbed state, if they experience steric hindrances that prevent them from the ideal orientation needed to adsorb. In the current

experiments, the concaved interface may result in the sterically suppressed adsorption rate if the surfactant is in the inner phase. In general, the adsorption rate constant should not be dependent on surfactant concentration below CMC. However, the values of the rate constants shown in **Table 7** do have a CMC dependence. Here, there are two concentrations used for each surfactant, one is above the CMC and the other is below CMC. Above CMC, the time scale of the kinetic adsorption may be affected the demicellization process of those micelles that occurs before the surfactant molecules adsorbed onto the interface. In particular, the decrease in adsorption rate of detergent mix is much greater than that of AES when surfactant concentration is above CMC. This may be caused by the mixture of micelles in detergent mix that form more appreciably affecting the surfactant adsorption.

In addition to the bilgewater system with NSBM#4 as the oil phase and SSW as the aqueous phase, model systems are also investigated. Particularly, the model system uses LMO and distilled water, with the model surfactants, TritonX-100 and SDS, and commercial surfactants, Type 1, Solid Surge, and PRC, added to the water. The calculated values of those surfactant are listed in **Table 8**. In particular, we use the Frumkin isotherm model with the interaction parameter, K. As shown in **Table 8**, the maximum surface coverage of all the surfactants are within the appropriate order of magnitude, while the adsorption constant for Solid Surge and PRC are larger than the others. However, the adsorption rate constant for these two surfactants are smaller than that of the other surfactants. In addition, the diffusivity of these two surfactants are much lower than the order of magnitude of typical surfactant molecules O(10^{-10}). One possible reason for this deviation is that both Solid Surge and PRC have multiple surfactants such that the molecular weight used in the calculation is approximated values, which may result in imprecise data.

Table 8. Parameters for the model and commercial surfactants studied in Task 1, Deliverable 3

Surfactant	M_w (g/mol)	Γ_∞ (mol/m^2)	κ (m^3/mol)	K	D (m^2/s)	k_{ads} (m^3/mol · s)	k_{des} (s^{-1})	Type
TritonX-100	625	1.64E-06	1.41E+05	1.152	6.28E-11	42.548	0.0023	Non-ionic
SDS	288	2.81E-06	104.98	3.618	2.45E-11	53.8	2.7	Anionic
Type 1	616.82	1.88E-06	1.19E+05	0.3947	1.04E-10	31.83	4.11E-04	Non-ionic
Solid Surge	214.39	1.04E-06	4.04E+06	0.3587	3.40E-12	5.59	2.68E-06	Non-ionic
PRC	293.38	1.00E-06	2.10E+06	1.341	9.50E-14	1.73	2.80E-06	Non-ionic + Anionic

The calculated data of κ and k_{ads} listed in **Table 6**, **7** and **8** are also compared to that of other commonly used surfactants as shown in **Figure 17** and **18**, respectively. Particularly, κ of Type 1, TritonX-100, PRC and Solid Surge are relatively higher than that of other surfactants, while the adsorption rate constant, k_{ads}, calculated values of the surfactants used in this task are within the broad range of values reported for other surfactants. The k_{ads} of AES and detergent mix are higher than most of the surfactants reported in the literatures close to that of Heptanol and Octanol, which is generally around or below 10^1.

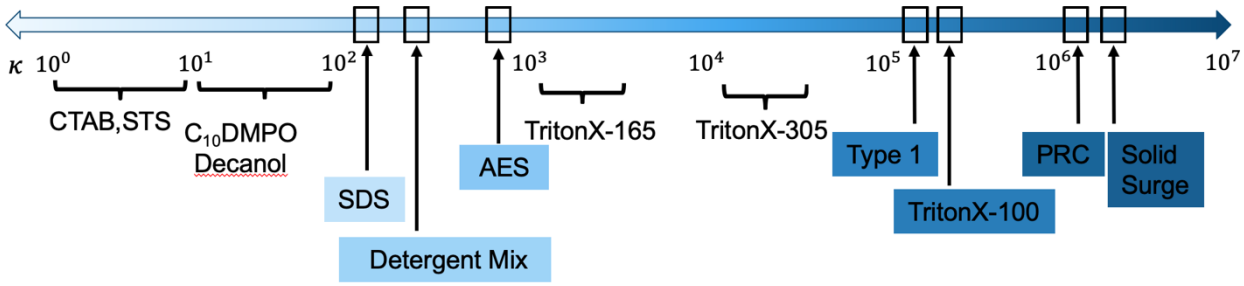

Figure 17. Comparison of κ for the calculated surfactants with other commonly used surfactants. The larger the κ, the more the surfactant tends to reduce the IFT.

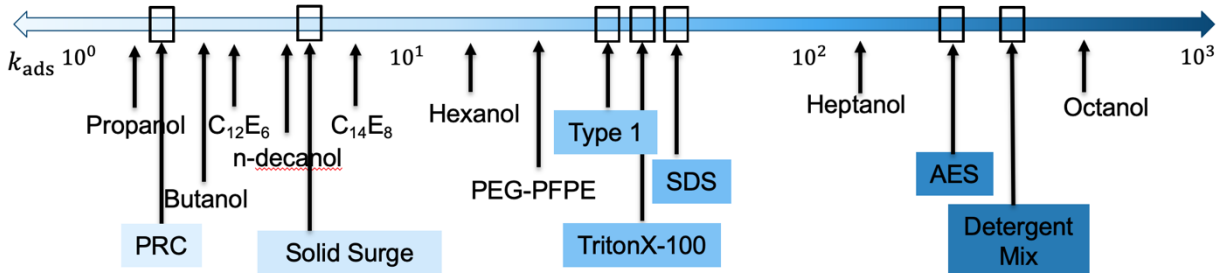

Figure 18. Comparison of adsorption rate constant, k_{ads}, of calculated surfactants with other commonly used surfactants.

Task 1, Objective 4: Droplet Coalescence and Film Drainage Time

Preliminary tests of droplet trap/coalescence has been performed for mineral oil droplet in water using 4-channel Stokes' trap device, towards the completion of Task 1, Deliverables 4. Three systems were performed for droplet coalescence experiments. 1) Distilled water in NSBM#4 with detergent mix surfactant; and Distilled water in light mineral oil with 2) detergent mix and 3) Type 1 commercial surfactant. Film drainage time has also been analyzed for those coalesced droplets cases. In the first system, detergent mix of 0 ppm, 10 ppm and 100 ppm were tested. The results show no coalescence even without added detergent mix. Possible reasons could be the surfactants in the outer phase such that the Marangoni stress at the interface cannot be damped. Also, the droplets contact time may be insufficient for the film to drain, which requires better control of the droplet trapping. For the second system, 10 ppm and 100 ppm detergent mix were tested, and both show droplet coalescence. The film drainage times were analyzed as shown in **Figure 19 (a)**. Clearly, the droplets coalesce immediately after they are in contact with each other. For the third system, 50 ppm and 100 ppm Type 1 were used, and the film drainage time is shown as **Figure 19 (b)**. It took about ~0.88 s for 100 ppm and ~1.48s for 50 ppm. The possible reason that it took a little longer for the droplet to coalesce at 100 ppm is that the incoming droplet rotates about the trapped droplet when they are in contact with each other, which may increase the film drainage time slightly. Based on the current preliminary results from system 2 and 3 tested here, the Type 1 may be better for stabilizing the droplets as compared to detergent mix. This needs to be justified

for further experiments. The current Stokes Trap experiments have proved successful coalescence of droplets for water-in-mineral oil system.

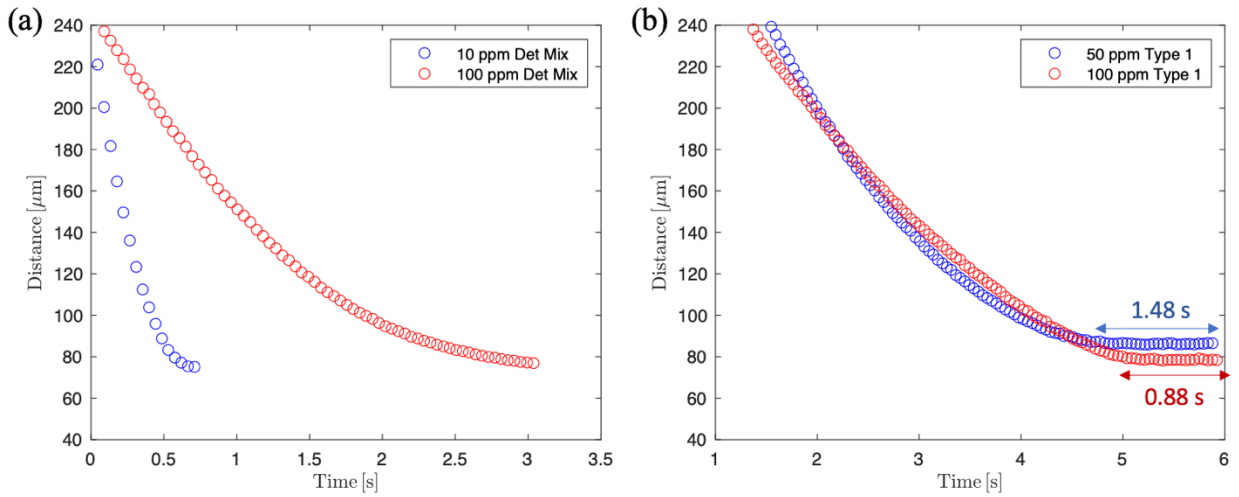

Figure 19. (a) Film drainage time of droplet coalescence for distilled water in LMO with 10 ppm and 100 ppm detergent mix in water. Both cases show immediate coalescence when the droplets are in contact with each other. (b) Film drainage time of droplet coalescence for distilled water in LMO with 50 ppm and 100 ppm commercial surfactant Type 1 in water. Both show the film drainage time of around 1 second.

Task 2, Objective 1: Static Bulk Emulsion Stability Test

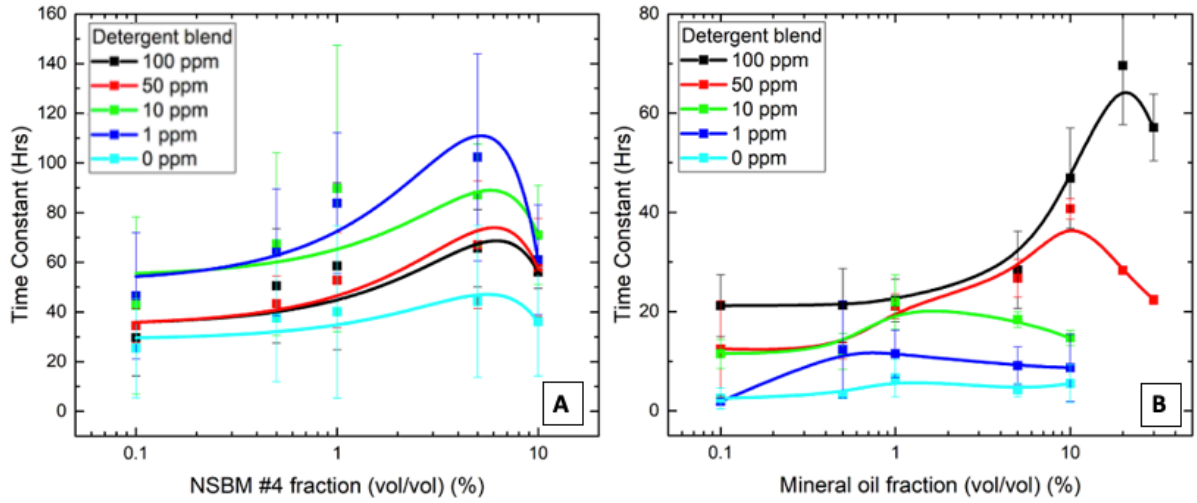

Figure 20. (A) Plots of exponential decay time constant for the NSBM#4 system, varying with oil fraction. Low values of the time constant correspond to a rapidly destabilizing system, while high values of the time constant correspond to slow destabilization. The plots show the trend of increasing stability with oil fraction until 10% oil is reached. The curves here are quadratic best

fits. (B) Plots of exponential decay time constant for the light mineral oil system, varying with oil fraction, showing the trend of increasing stability with oil fraction, a peak is reached. The peak location is dependent on surfactant concentration.

Two oil-water systems were investigated to study the bulk emulsion stability. The first one is to use NSBM#4 in distilled water with detergent blend as surfactant, the other is to use light mineral oil in distilled water with detergent blend. There are two parts of the results reported here. First, stability tests for time constant versus o:w ratio of 0.1%, 0.5%, 1%, 5%, 10% with detergent blend of 1 ppm, 10 ppm, 50 ppm, 100 ppm were reported (See **Figure 20**). In particular, the timescales associated with the destabilization time are extracted using an exponential function fitted to the time-dependent emulsion turbidity plot based on the processed images from the centrifuge tube tests. The time constant versus o:w ratio shows a general non-monotonic trend with a peak in stability around 5% for NSBM#4, while there is a surfactant concentration dependent peak location for mineral oil. Here, we have addressed this non-monotonic stability behavior as a result of multiple components. The initial increase in the stability is due to the collision with slower smaller droplets that impeded droplet creaming rates. For the decrease in the stability, there are two combined factors. The first is the surface area-driven phenomenon. The increase of the total amount of the oil in the emulsion causes the increase of the droplets interfacial area, such that the surfactant molecule coverage lowers leading to the increase of IFT. This increasing IFT enhance the coalescence between droplets and then decrease the droplet stability. The second factor is the collision-driven effect. The higher total number of droplets causes more collisions between the droplets and therefore enhances the coalescence that induces a faster creaming rate. The peak location of the time constant that is fixed at around 5% o:w for NSBM#4 cases is likely due to the surfactants present in the NSBM#4 phase, which also stabilizes the interface.

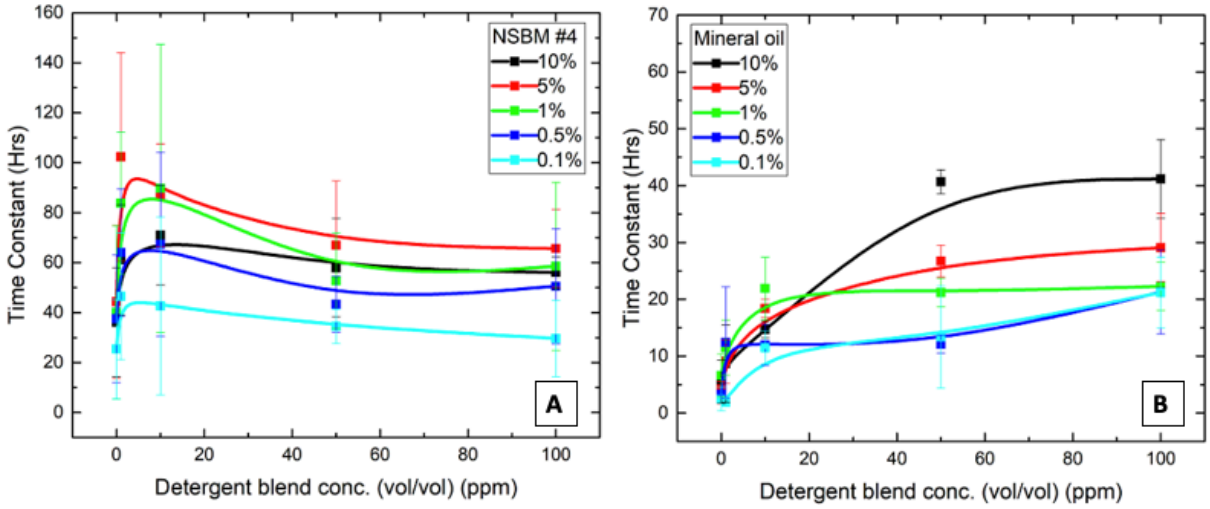

Figure 21. (A) Plots of exponential decay time constant for the NSBM#4 system, varying with surfactant concentration, showing the non-monotonic trend in stability to creaming with surfactant concentration. (B) Plots of exponential decay time constant for the light mineral oil system, varying with surfactant concentration, showing the much more plateau-like trend in stability plotted against surfactant concentration, as compared to non-monotonic NSBM#4 results. The curves here are spline fits.

Second, the same time constants are plotted versus the surfactant concentration at various o:w ratio (see **Figure 21**) Here, there is a sharp increase of the stability as a function of surfactant concentration up to CMC for NSBM#4 system, which is due to the increased surfactant coverage at the interface. However, in the mineral oil case, the stability then reaches a plateau after the CMC, while there is a slight decrease of stability for the NSBM#4 case. This is addressed due to the fact that the micelles of detergent blend are able to swell minuscule amount of oil entrained at the center. These very small, stable oil droplets are not large enough to affect the turbidity. On the other hand, the mineral oil is insoluble to the detergent blend such that there is no change of stability above CMC.

Particle size analysis was also performed with different aqueous emulsions containing SERDP oil, using a BlueWave Laser Diffraction Particle Size Analyzer. The five different samples were conducted at 0.1%, 0.5%, 1%, 5%, and 10% oil. The samples contained 0 ppm in **Figure 22** (left) and 100 ppm in **Figure 22** (right) of the SERDP-recommended detergent blend. As expected, at the fixed detergent concentration the droplet sizes were consistently in the same size range, for a given surfactant concentration. In addition, when 100 ppm detergent mix is added, the number of small size droplets are increased, which indicates the enhanced stabilization of the emulsion. Similar experiments were performed for each of the same five oil:water ratios for 0, 1, 10, and 50 ppm of the recommend SERDP blend surfactants as well as 100 ppm LAS model surfactants. The majority of the droplets for all the systems studied were between 1-10 micrometers.

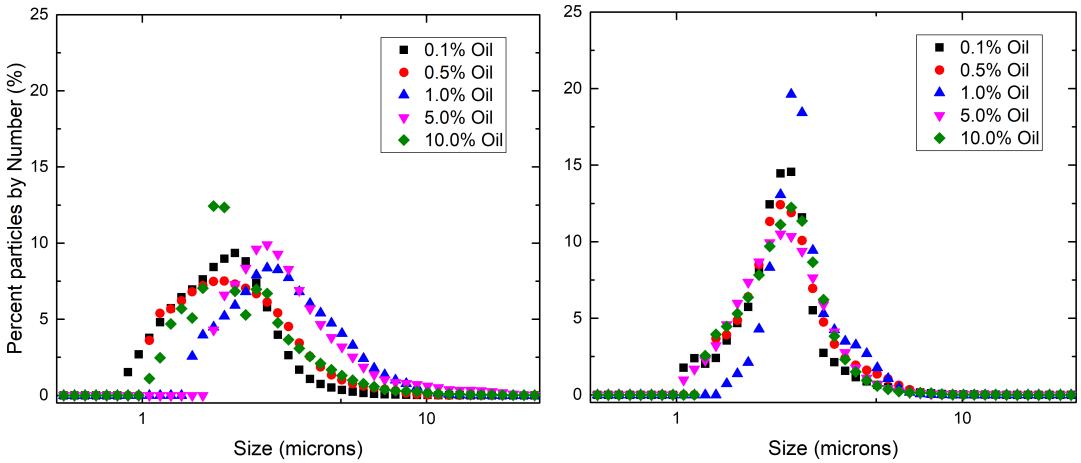

Figure 22. Number size distribution of the droplets in the emulsion with (left) no surfactant and (right) 100 ppm of the SERDP recommended detergent mix. In general, the presence of surfactant shows increase in the number of small size droplets, as expected.

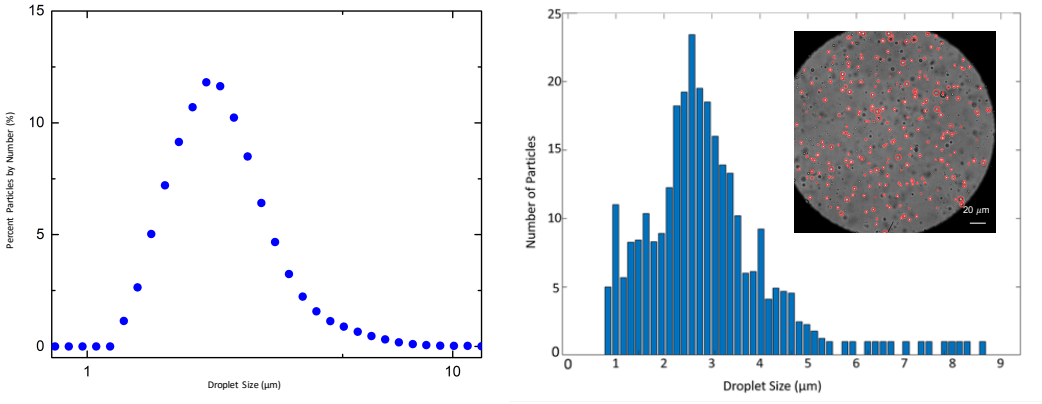

Figure 23. Number size distribution of droplets in the emulsion (0.1% Oil, 100 ppm detergent mix) measured from (left) Laser Diffraction compared to (right) Microscopy. Results from both measurements are consistent to each other, and show the size of droplets are between 1~10 µm. The inset shows the edge detection of the droplets using Matlab in a microscopy image.

Custom-designed extra-shallow PDMS wells were fabricated to allow microscopy images of emulsion samples to be taken with high magnification lenses of very short focal lengths. Microscopy images are recorded for every sample tested in stability and rheology tests. Custom Matlab code was written to identify and calculate the diameters of imaged droplets and generate particle size distributions from this data. The results compare well with the size distribution from laser diffraction (**Figure 23**). Both methods confirm the findings of number size distributions of the laser diffraction results—that the majority of particles are of the order of 1 micrometer in diameter, while almost all are below 10 micrometers in diameter.

Multiple stability tests were conducted on several emulsion recipes designed to test the impact of adding salt to our base emulsion system and model emulsion system. This was done to compare the stability test results for an emulsion system under ideal conditions for surfactant effectiveness with a system under conditions (like seawater) known to impact surfactant performance. The tests were conducted for samples of all five relevant oil:water (o:w) ratios, at 100 ppm of SERDP surfactant blend for both in a bulk phase of commercially available simulated seawater (SSW), for dispersed phases of both NSBM#4 and light mineral (model) oil. Repetition of these stability tests was completed to ensure repeatability of results and collect average decay time constants for data analysis purposes. The stability of droplets as a function of their size distribution was also explored. Laser diffraction particle size analysis was performed for each unique emulsion sample, across all tests, at both the start and end of the stability test in order to probe aging behavior.

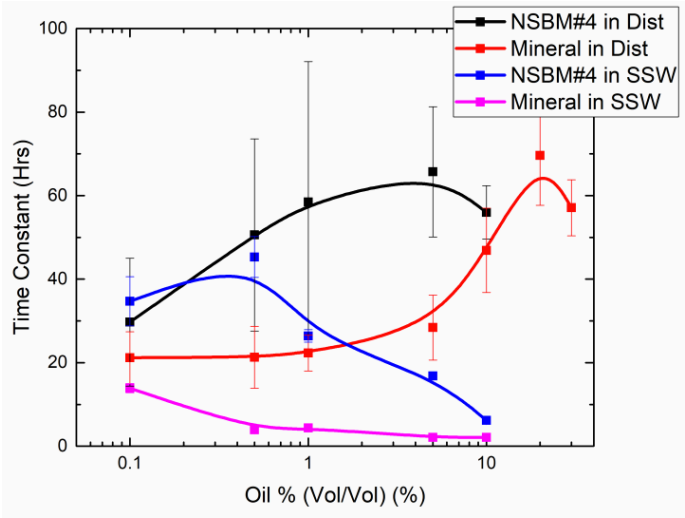

Figure 24. A plot of emulsion destabilization time against o:w for multiple systems of 100 ppm SERDP detergent mix emulsions. This figure shows the clear impact on emulsion stability of adding salt, and also shows how (at least for low o:w) mineral oil systems are more impacted by the addition of salt than NSBM#4 systems.

The addition of simulated seawater was found to impact the surfactant performance, as expected, but especially so for high o:w ratios. The average time decay constants for both 0.1% NSBM#4 and 0.1% mineral oil in SSW were found to be similar to those found for their distilled-water counterparts. However, the destabilization times for mineral oil in SSW rapidly decayed for all o:w ratios measured above 0.1%, and destabilization times for NSBM#4 in SSW rose slightly to a peak near 0.5% o:w and decayed steadily thereafter, reaching very low levels at 10% o:w. See **Figure 24** for an illustration of these results. The increased susceptibility of mineral oil emulsions to the surfactant-deteriorating effects of adding salt is hypothesized to be a result of NSBM#4's solubility to some surfactants, a phenomenon which allows NSBM#4 droplets to be partially stabilized internally, where salt is not present.

Task 2, Objective 2: Simple-shear Bulk Emulsion Viscosity Measurement

Rheometry was performed on simulated bilge emulsion samples of 0.1%, 0.5%, 1%, 5%, and 10% oil in water (o:w) ratios at 100, 50, and 10 ppm of SERDP surfactant blend and 100 ppm LAS model surfactant, as well as 10% o:w at 1 ppm surfactant. **Figure 25** shows examples of 0.5% oil with 10 ppm detergent mix. For all samples with o:w ratios oil or below, the viscosity plateaus at a value slightly above that of water, and independent of shear rate (exhibiting Newtonian-like behavior). The front sweeps (low-to-high shear rate) and back sweeps (high to low shear rates) for all of these samples yielded the same results. However, for all samples with 10% oil, a hysteresis effect was observed. It is suspected that this is because of destabilization of high o:w emulsions, leading to increased creaming of the oil phase. Laser diffraction and microscopy particle size distributions support this hypothesis. To isolate the critical oil% for the onset of hysteresis, further experiments were performed with oil percent of 6%, 7%, 8%, 9%, 9.5%, 10%, and 11%, with the critical value of 10% oil found for these samples.

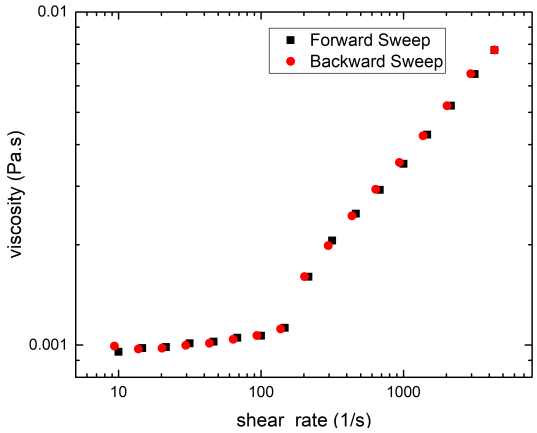

Figure 25. Steady-shear viscosity of (left) 0.5 % NSBM#4 oil with 10 ppm detergent mix, as a function of shear rate. In general, regions constant viscosity are observed for low to moderate shear rates, depending on the sample. The appearance of shear thickening (increase in viscosity with shear rate) at high shear rates is due to flow instabilities and are an artifact of the measurement. Chemical compositions with 10% oil or greater show hysteresis behavior, due to emulsion destabilization.

In order to test the hypothesis of hysteresis in 10% and higher o:w systems being caused by destabilization of high oil fraction samples at high shear rates, particle size distribution techniques were employed. Laser diffraction particle size analysis was performed on all samples from before and after the rheology experiments. Shifts in the size distribution were not observed for o:w ratios of 1% or less but were observed for the 10% oil system as shown in **Figure 26**.

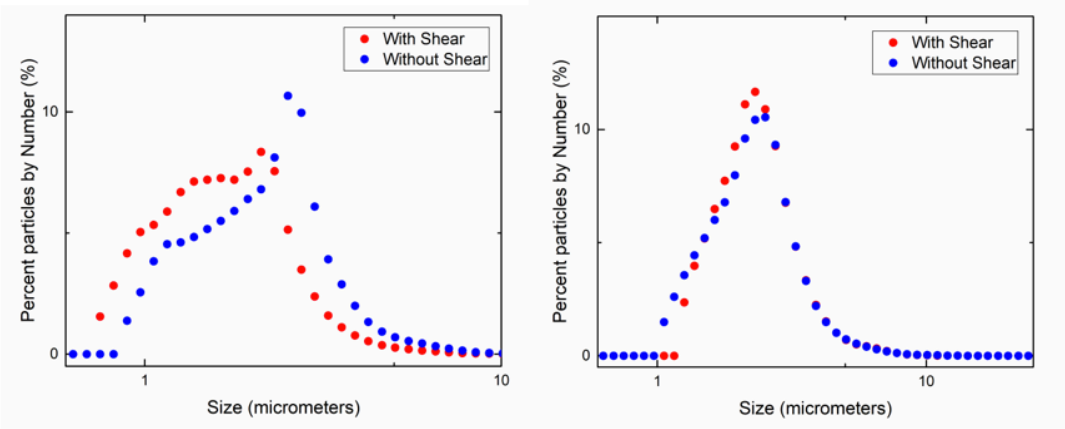

Figure 26. Before and after rheometry laser diffraction particle size distributions for 10% (left) and 0.1% (right) NSBM#4 emulsion samples. Both these samples have 10 ppm surfactant. The shift in the distribution after shear for the 10% o:w sample is evidence a decrease in number of larger droplets due to creaming during high-speed destabilization.

Task 2, Objective 3: Pre-prepared Emulsion Stability Test in TC Flows

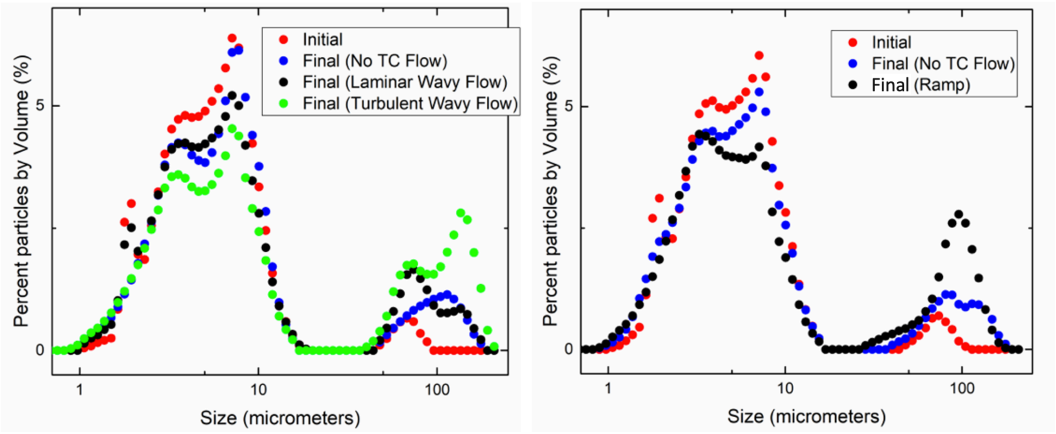

Figure 27. Pre-prepared emulsion of 0.1% NSBM#4 oil in water with 100 ppm detergent mix tested in Taylor-Couette cell for (left)"step-wise" and (right) "ramped" flow condition. Both show decreases in the number of droplets of size less than 10 micrometers and corresponding increase in droplets of size on the order of 100 microns occurred with time, due to emulsion destabilization.

Experiments were performed on large volumes of 0.1% o:w, 100 ppm surfactant simulated bilge emulsion using a custom-built Taylor-Couette Cell. In the first type of experiment, the emulsion mixture was held at a low-mixing Laminar Wavy Flow (LWF) state for ten minutes, and then brought to a high-mixing Turbulent Wavy Flow (TWF) for an additional ten minutes. Samples were drawn at the start, after undergoing LWF, and after undergoing TWF, and sent for laser diffraction particle size analysis. In the second type of experiment, a pre-prepared emulsion mixture was "Ramped" gradually up through a series of flow states of increasing mixing intensity. Samples were taken at the start and after undergoing the Ramp process and sent for laser diffraction particle size analysis. Representative results of both types of experiment are shown in **Figure 27**. A decrease in droplets of a size less than 10 micrometers and a corresponding increase in droplets of size on the order of 100 microns occurred with time, likely due to emulsion destabilization – similar to that observed in traditional vial tests. This destabilization effect was more pronounced in a sample that underwent the "ramp" Taylor-Couette test, due to enhanced destabilization from the flow. Similar shifts in size distributions were not observed in 0.1% o:w samples with rheometry alone (Objective 2), and are suggestive of the importance of the flow and mixing types in emulsion destabilization and can be used to inform conditions for liquid-liquid separation technologies.

Experiments were performed on large volumes of various recipes of emulsion mix using the same TC Cell. Two types of experiment were performed. The first experiment type was a repletion of our previous base TC cell experiment, with emulsion mixtures held at a low-mixing LWF state held for ten minutes followed by a high-mixing TWF for an additional ten minutes. The experiment was conducted on emulsions of NSBM#4 and light mineral (model) oil in a bulk phase of SSW for the first time (see **Figure 28**). The experiments also showed a decrease in droplets of a size on the order of 10 micrometers and an increase in the number of droplets of a size on the order of 100 micrometers. The additional of salt (SSW) to the tests saw results that were similar in kind but different in degree. For instance, mineral oil in SSW emulsion systems saw a more dramatic decrease in droplets ~10 micrometers and an accompanying relative increase in droplets ~1 micrometer, owing to the increased instability of addition salt to a mineral oil system.

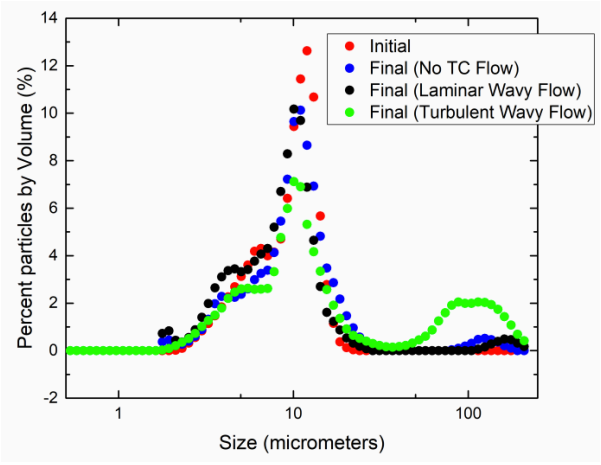

Figure 28. Pre-prepared emulsion of 0.1% NSBM#4 in SSW with 100 ppm detergent mix in Taylor-Couette cell for "step-wise" flow condition.

The second experiment type was identical to the first with the addition of a third step: emulsions being held at a very-high-mixing Turbulent Taylor Vortex Flow (TTF) for an additional ten minutes. This test was intended to determine if additional mixing strength had an additional effect on change in droplet size distributions. This second experiment type was conducted for NSBM#4 in both distilled water and SSW, and for light mineral oil in both distilled water and SSW. All experiments conducted had 0.1% o:w and 100 ppm SERDP detergent blend. The addition of ten minutes of TTF to all four systems was not found to cause a significant difference in changes to the droplet size distributions over exposure to only LWF and TWF, suggesting that there are diminishing returns to increasing mixing speed beyond the point of initial turbulence.

Task 2, Objective 4: In-situ Emulsion Formation and Stability

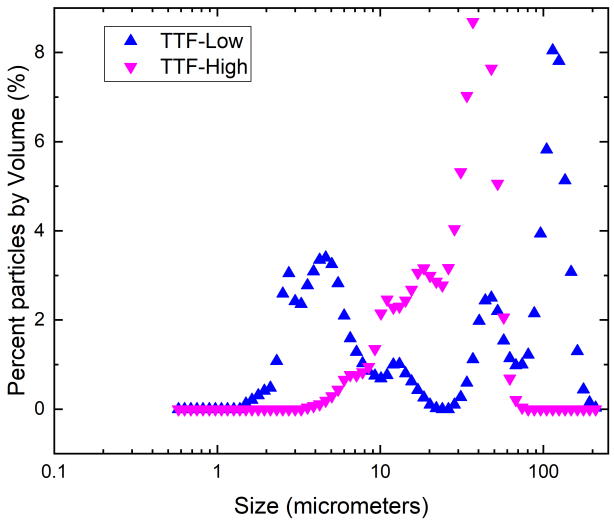

Figure 29. Droplet size distribution by volume for 2% NSBM#4 & 100 ppm SERDP system for experiment performed in Taylor Couette cell, The peak shifts to right towards higher droplet size with reduction in mixing speeds.

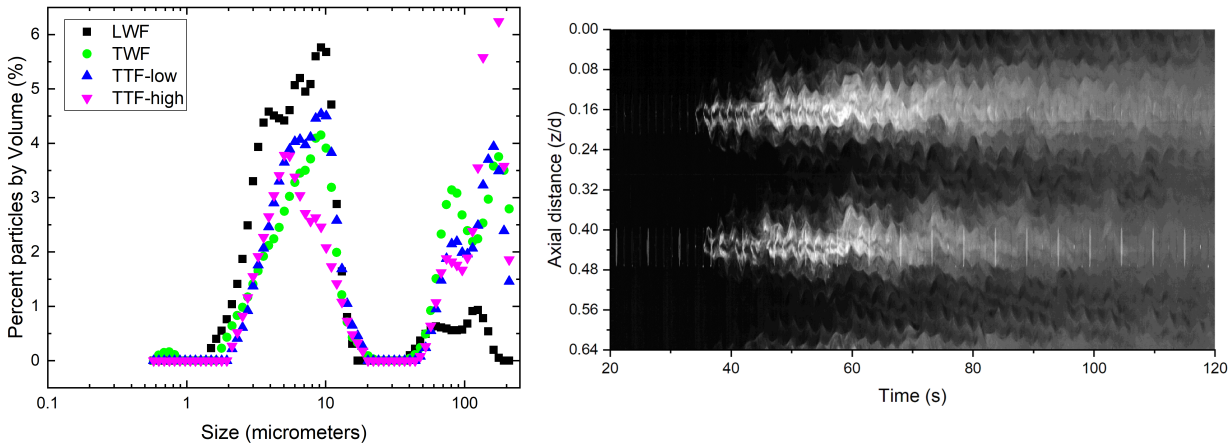

(a) (b)

Figure 30. (a) Droplet size distribution by volume for 0.1 % NSBM#4 & 100 ppm SERDP emulsion system made from concentrated 1% NSBM#4 emulsion formed in homogenizer and final mixing is performed in Taylor Couette cell (b) Representative example of Space-time plot for in-situ injected concentrated emulsion into the Taylor wavy vortices in the TC experiments

Following the pre-preprared emulsion stability test, the preliminary in-situ emulsion formation and stability were investigated with 5 sets of experiments. The purpose of these 5 sets of experiments described in the Technical Approach was to determine the best possible way to study the formation and mixing of stable emulsions in TC cell. The emulsion was loaded into the TC cell to observe the effect of stepped mixing speed on the size distribution of droplets and overall mixing in the solution. The results from the first experiments showed that unlike light mineral oil, NSBM#4 was able to form emulsions at lower shear rates available in the jar tests and the TC cell. It was shown in the droplet size distribution obtained from laser diffraction analysis that the peak of droplet size shift to the right towards larger droplets as the mixing speed is reduced from high (TTF) to low (TWF). At the lowest speed (LWF) the oil droplets seem to have destabilized and separated from the solution by moving to the top of the cylinder, which was confirmed by the absence of detection signal in the laser diffraction and visible droplets in optical microscopy. It can be concluded from the second TC experiment that there was some degree of emulsification at highest shear rates (mixing speed) but as soon as the mixing speed was reduced, the oil droplets in the solution destabilized and separated out from the solution. The effects of higher oil concentration, up to 2% oil, were further probed the study showed results **Figure 29**, showing similar results. Finally, the results **Figure 30** showed that a peak formed at the smaller droplet size in the solution, which reduces with increasing mixing speed and a second peak at larger droplet size increases with higher mixing speeds. The formation of a peak at higher mixing speed shows the effects of droplet coalescence due to shear in the flow. As a part of this work, we were also able to visualize the mixing of concentrated emulsion into the water-surfactant solution in different flow conditions at the beginning of the experiments, which will be used to study mass transfer and dispersion coefficients of these emulsion systems.

Conclusions and Implications for Future Research

For the study of microscale droplets from Task 1, first, the hydrophilic surface treatment for PDMS microfluidic devices was performed. The method optimized the use of plasma and pre-treatment of the devices. The treatment was found to be successful, and devices were able to run experiments for oil-in-water systems for both dynamic IFT measurement and Stokes trap. Second, the dynamic IFT measurements of both microfluidic and pendant drop methods were performed for bilgewater systems with both oil-in-water and water-in-oil systems using detergent mix or model surfactant AES added to the water. The results showed that the IFT decays much faster when surfactant and water is in the outer phase and oil in the inner phase for micro-scale droplets, while the rate of decay does not change significantly for milli-scale droplets. In addition, dynamic IFT measurements in both microfluidic and pendant drop for model systems with light mineral oil in distilled water with other model and commercial surfactants were also performed. Third, characterization of surfactant molecules was performed using isotherm models and surfactant transport equations. In particular, the adsorption constant, κ, maximum surface coverage, Γ_∞, surfactant diffusivity, D, and adsorption/desorption rate constants, were calculated and compared to other typical surfactants. Most of the values extracted are within the reasonable range, except for the commercial surfactants with imprecise molecular weight. The results of these studies were published in Chen and Dutcher Soft Matter (2020) [35] and collaborative paper with Naval Research Laboratory, Church et al. (Journal of Water Process Engineering) (2020) [38]. Finally, Stokes' trap devices were used to perform droplet coalescence experiments. Preliminary results have shown the successful trapping and coalescence of the droplets, particularly for water-in-oil systems. The results and conclusions based on all four of the Task 1 objectives have been written up for an invited manuscript, currently under review with Langmuir. In addition, the results of this work have laid the foundation of systematic studies of surfactant transport for both bilgewater and fire-fighting foam systems, in follow up grant SERDP WP19-1407.

For the macroscale bulk emulsion experiments in Task 2, first, static (no-flow) emulsion stability tests were performed. The study found non-monotonic relationships for emulsion destabilization times with both o:w ratio and surfactant concentration, showing stabilization of emulsion depending on the amount of oil and surfactant, respectively. In some cases, the appearance of spontaneous emulsification of observed during microscopy of the droplet system, with results written up in a co-authored review paper Narayan et al. COCIS (2020) [39]. Second, the viscosity of the bulk emulsion was measured using a shear rheometer. Hysteretic behavior was observed in the steady-shear viscosity measurement, and evolution of the particle size distributions where observed for high oil-in-water ratio emulsions (>9.0% oil), due to bulk destabilization and increased creaming of the oil phase. Third, emulsion destabilization was observed after the pre-prepared emulsion underwent the Taylor-Couette flow test. Changes in particle size distributions were observed even for low oil content samples (0.1% oil). The results have implications for methods used to destabilize and separate emulsions on ships, even for low oil content systems. Finally, in-situ injection of oil and oil emulsions into the TC cell during mixing, enabled observations of the formation and mixing of emulsions, and has provided a framework for further exploration to study mixing dynamics of oil-water emulsion in different flow conditions.

Literatures Cited

[1] J. Church, J. G. Lundin, D. Diaz, D. Mercado, M. R. Willner, W. H. Lee and D. M. Paynter, "Identification and characterization of bilgewater emulsions," *Science of the Total Environment,* vol. 691, pp. 981-955, 2019.

[2] H. Eskandarloo, M. J. Selig and A. Abbaspourrad, "In situ H2O2 generation for de-emulsification of fine stable bilge water emulsions," *Chemical Engineering Journal,* vol. 335, pp. 434-442, 2018.

[3] J. Church, D. M. Paynter and W. H. Lee, "In Situ Characterization of Oil-in-Water Emulsions Stablized by Surfactant and Salt Using Microsensor," *Langmuir,* vol. 33, no. 38, pp. 9731-9739, 2017.

[4] B. K. Korbahti and K. Artut, "Electrochemical oil/water demulsification and purification of bilgewater using Pt/It electrodes," *Desalination,* vol. 258, no. 1, pp. 219-228, 2010.

[5] S. M. Emadian, M. Hosseini, M. Rahimnejad, M. H. Shahavi and B. Khoshandam, "Treatment of a low-strength bilge water of Caspian Sea ships by HUASB technique," *Ecological Engineering,* vol. 82, pp. 272-275, 2015.

[6] A. Moslehyani, M. Mobaraki, A. F. Isloor and M. H. Othman, "Photoreactor-ultrafiltration hybrid system for oily bilge water photooxidation and separation from oil tanker," *Reactive and Functional Polymers,* vol. 101, pp. 28-38, 2016.

[7] N. Wilkinson and C. Dutcher, "Taylor-Couette flow with radial fluid injection," *Review of Scientific Instruments,* vol. 88, no. 8, p. 083904, 2017.

[8] A. Metaxas, N. Wilkinson, E. Raethke and C. Dutcher, "In Situ polymer flocculation and growth in Taylor-Couette flows," *Soft Matter,* vol. 14, no. 42, pp. 8627-8635, 2018.

[9] N. Wilkinson and C. Dutcher, "Axial mixing and vortex stability to in situ radial injection in Taylor-Couette laminar and turbulent flow," *Journal of Fluid Mechanics,* vol. 854, pp. 324-347, 2018.

[10] D. Woytowich, C. W. Dalrymple and M. Britton, "Electrocoagulation (CURE) treatment of ship bilgewater for the US Coast Guard in Alaska," *Marine Technology Society Journal ,* vol. 27, no. 1, pp. 62-67, 1993.

[11] G. Potters, Dr. Geert Potters & bookboon.com, 2013.

[12] K. Karakulski, A. Kozlowski and A. Morawski, "Purification of oily wastewater by ultrafiltration," *Separations Technology,* vol. 5, no. 4, pp. 197-205, 1995.

[13] I. Ivanov and P. Kralchevsky, "Stability of Emulsions under Equilibrium and Dynamic Conditions," *Colloids Surfaces A Physicochem. Eng. Asp.,* vol. 128, no. 1-3, pp. 155-175, 1997.

[14] B. Binks and C. Whitby, "Nanoparticle Silica-Stabilised Oil-in-Water Emulsions: Improving Emulsion Stability," *Colloids Surfaces A Physicochem. Eng. Asp.,* vol. 253, no. 1, pp. 105-115, 2005.

[15] T. Tadros, Emulsion Formation and Stability, Weinheim, Germany: Wiley-VCH Verlag GmbH & Co., 2013.

[16] P. Walstra, Encyclopedia of Emulsion Technology, New York: Marcel Dekker, Inc, 1996.

[17] I. Kobayashi, S. Mukataka and M. Nakajima, "Production of Monodisperse Oil-in-Water Emulsions Using a Large Silicon Straight-Through Microchannel Plate," *Industrial & Engineering Chemistry Research,* vol. 44, no. 15, pp. 5852-5856, 2005.

[18] H. Tanaka, S. Yamamoto, A. Nakamura, Y. Nakashoji, N. Okura, N. Nakamoto, K. Tsukagoshi and M. Hashimoto, "Hands-Off Preparation of Monodisperse Emulsion Droplets Using a Poly(dimethylsiloxane) Microfluidic Chip for Droplet Digital PCR," *Analytical Chemistry,* vol. 87, no. 8, pp. 4134-4143, 2015.

[19] Y. Zhu, X. Pei, J. Jiang, Z. Cui and B. P. Binks, "Responsive Aqueous Foams Stabilized by Silica Nanoparticles Hydrophobized in Situ with a Conventional Surfactant," *Langmuir,* vol. 31, no. 47, pp. 12937-12943, 2015.

[20] R. Mikula, "Emulsion Characterization," *Advances in Chemistry,* vol. 231, pp. 79-129, 1992.

[21] L. M. Foster, A. J. Worthen, E. L. Foster, J. Dong, C. M. Roach, A. Metaxas, C. D. Hardy, E. S. Larsen, J. A. Bollinger, T. M. Truskett, C. W. Bielawski and K. P. Johnston, "High Interfacial Activity of Polymers "Grafted through" Functionalized Iron Oxide Nanoparticle Clusters," *Langmuir,* vol. 30, no. 34, pp. 10188-10196, 2014.

[22] S. H. Tan, N. T. Nguyen, Y. C. Chua and T. G. Kang, "Oxygen plasma treatment for reducing hydrophobic of a sealed polydimethylsiloxance microchannel," *Biomicrofluidics,* vol. 4, no. 3, p. 032204, 2010.

[23] S. D. Hudson, J. T. Cabral, W. J. J. Goodrum, K. L. Beers and E. J. Amis, "Microfluidic Interfacial Tensiometry," *Applied Physics Letters,* vol. 87, no. 8, p. 081905, 2005.

[24] C. Dong, C.-T. Hsu, C.-Y. Chiu and S.-Y. Lin, "A Study on Surfactant Adsorption Kinetics: Effect of Bulk Concentration on the Limiting Adsorption Rate Constant," *Langmuir,* vol. 16, no. 10, pp. 4573-4580, 2000.

[25] Y. He, P. Yazhgur, A. Salonen and D. Langevin, "Adsorption–desorption kinetics of surfactants at liquid surfaces," *Advances in Colloid and Interface Science,* vol. 222, pp. 377-384, 2015.

[26] N. J. Alvarez, W. Lee, L. M. Walker and S. L. Anna, "The effect of alkane tail length of CiE8 surfactants on transport to the silicone oil-water interface," *Journal of Colloid and Interface Science,* vol. 355, no. 1, pp. 231-236, 2011.

[27] N. Alvarez, L. Walker and S. Anna, "Diffusion-limited adsorption to a spherical geometry: The impact of curvature and competitive time scales," *Physical Review E,* vol. 82, no. 1, p. 11604, 2010.

[28] J. Eastoe and J. Dalton, "Dynamic surface tension and adsorption mechanisms of surfactants at the air-water interface," *Advances in Colloid and Interface Science,* vol. 85, no. 2, pp. 103-144, 2000.

[29] A. F. Ward and L. Tordai, "Time-Dependence of Boundary Tensions of Solutions I. The Role of Diffusion in Time-Effects," *The Journal of Chemical Physics,* vol. 14, no. 7, pp. 453-461, 1946.

[30] H. Manikantan and T. M. Squires, "Surfactant dynamics: Hidden variables controlling fluid flows," *Journal of Fluid Mechanics,* vol. 892, pp. 1-115, 2020.

[31] N. Alvarez, D. Vogus, L. Walker and S. L. Anna, "Using bulk convection in a microtensiometer to approach kinetic-limited surfactant dynamics at fluid–fluid interfaces," *Journal of Colloid and Interface Science,* vol. 372, no. 1, pp. 183-191, 2012.

[32] Q. Brosseau, J. Vrignon and J.-C. Baret, "Microfluidic Dynamic Interfacial Tensiometry (μDIT)," *Soft Matter,* vol. 10, no. 17, pp. 3066-3076, 2014.

[33] T. Trantidou, Y. Elani, E. Parsons and O. Ces, "Hydrophilic surface modification of PDMS for droplet microfluidics using a simple, quick, and robust method via PVA deposition," *Microsystems & Nanoengineering,* vol. 3, p. 16091, 2017.

[34] L. G. Rigat-Brugarolas, A. Homs-Corbera and J. Samitier, "Highly hydrophilic microfluidic device prototyping using a novel poly(dimethylsiloxane)-based polymeric mix," *RSC Advances,* vol. 5, pp. 7423-7425, 2015.

[35] Y. Chen and C. S. Dutcher, "Size dependent droplet interfacial tension and surfactant transport in liquid-liquid systems, with applications in shipboard oily bilgewater emulsions," *Soft Matter,* vol. 16, pp. 2994-3004, 2020.

[36] S. Narayan, D. B. Moravec, B. G. Hauser, A. J. Dallas and C. S. Dutcher, "Removing Water from Diesel Fuel: Understanding the Impact of Droplet Size on Dynamic Interfacial Tension of Water-in-Fuel Emulsions," *Energy & Fuels,* vol. 32, no. 7, pp. 7326-7337, 2018.

[37] Y. Chen, S. Narayan and C. S. Dutcher, "Phase-Dependent Surfactant Transport on the Microscale: Interfacial Tension and Droplet Coalescence," *Langmuir,* 2020.

[38] J. Church, M. R. Willner, B. R. Renfro, Y. Chen, D. Diaz, W. H. Lee, C. S. Dutcher, J. G. Lundin and D. M. Paynter, "Impact of Interfacial Tension and Critical Micelle Concentration on Bilgewater Oil Separation," *Journal of Water Process Engineering,* 2020.

[39] S. Narayan, A. S. Metaxas, R. Bachnak, T. Neumiller and C. S. Dutcher, "Zooming in on the role of surfactants in droplet coalescence at the macro- and microscale," *Current Opinion in Colloid & Interface Science,* vol. 50, 2020.

Appendices

List of Scientific/Technical Publications

1. Y. Chen, S. Narayan, C.S. Dutcher, *Phase-dependent surfactant transport on the microscale: Interfacial tension and droplet coalescence*, Langmuir, 2020
2. J. Church, M.R. Willner, B.R. Renfro, Y. Chen, D. Diaz, W.H. Lee, C.S. Dutcher, J.G. Lundin, D.M. Paynter, *Impact of Interfacial Tension and Critical Micelle Concentration on Bilgewater Oil Separation*, Journal of Water Process Engineering, 2020
3. S. Narayan, A.E. Metaxas, R. Bachnak, T. Neumiller, and C.S. Dutcher, *Zooming in on the role of surfactants in droplet coalescence at the macro- and microscale,* Current Opinion in Colloid & Interface Science, 2020
4. Prof. Cari Dutcher presented a webinar for the SERDP & ESTCP Webinar Series on waste reduction and treatment in Armed Forces vessels, June 2020.

5. Y. Chen, C. S. Dutcher, *Size dependent droplet interfacial tension and surfactant transport in liquid-liquid systems, with applications in shipboard oily bilgewater emulsions,* Soft Matter, 16, 2020
6. Prof. Cari Dutcher gave an invited lecture *Understanding Shipboard Oil/Water Emulsions Using Macro- and Micro-scale Flows* for the Advancing Emulsion Science Session, SERDP/ESTCP Symposium 2019, Washington DC.
7. Dr. Yun Chen presented *Size dependent droplet interfacial tension and surfactant transport in oily bilgewater systems* at the American Physical Society - Division of Fluid Dynamics (APS – DFD) 72nd Annual Meeting, Seattle, WA, Nov 2019.
8. Dr. Yun Chen presented poster *Size dependent droplet interfacial tension and surfactant transport in liquid-liquid system* at the Mathematical Fluids, Materials, and Biology Conference 2019 at the University of Michigan, Ann Arbor, MI.
9. Dr. Yun Chen presented poster *Understanding Shipboard Oil/Water Emulsions Using Macro- and Micro-scale Flows* at the SERDP & ESTCP Symposium 2018, Washington, District of Columbia, USA.